NATIONAL ADVISORY COMMITTEE FOR AERONAUTICS

REPORT 1220

CALCULATIONS OF LAMINAR HEAT TRANSFER AROUND CYLINDERS OF ARBITRARY CROSS SECTION AND TRANSPIRATION-COOLED WALLS WITH APPLICATION TO TURBINE BLADE COOLING

By E. R. G. ECKERT and J. N. B. LIVINGOOD

1955

For sale by the Superintendent of Documents, U. S. Government Printing Office, Washington 25, D. C. Yearly subscription, $10; foreign, $11.25; single copy price varies according to size - - - - - - - - - Price 25 cents

REPORT 1220

CALCULATIONS OF LAMINAR HEAT TRANSFER AROUND CYLINDERS OF ARBITRARY CROSS SECTION AND TRANSPIRATION-COOLED WALLS WITH APPLICATION TO TURBINE BLADE COOLING

By E. R. G. ECKERT and J. N. B. LIVINGOOD

Lewis Flight Propulsion Laboratory
Cleveland, Ohio

National Advisory Committee for Aeronautics

Headquarters, 1512 H Street NW., Washington 25, D. C.

Created by act of Congress approved March 3, 1915, for the supervision and direction of the scientific study of the problems of flight (U. S. Code, title 50, sec. 151). Its membership was increased from 12 to 15 by act approved March 2, 1929, and to 17 by act approved May 25, 1948. The members are appointed by the President, and serve as such without compensation.

JEROME C. HUNSAKER, Sc. D., Massachusetts Institute of Technology, *Chairman*

LEONARD CARMICHAEL, PH. D., Secretary, Smithsonian Institution, *Vice Chairman*

JOSEPH P. ADAMS, LL. B., Vice Chairman, Civil Aeronautics Board.

ALLEN V. ASTIN, PH. D., Director, National Bureau of Standards.

PRESTON R. BASSETT, M. A., Vice President, Sperry Rand Corp.

DETLEV W. BRONK, PH. D., President, Rockefeller Institute for Medical Research.

THOMAS S. COMBS, Vice Admiral, United States Navy, Deputy Chief of Naval Operations (Air).

FREDERICK C. CRAWFORD, Sc. D., Chairman of the Board, Thompson Products, Inc.

RALPH S. DAMON, D. Eng., President, Trans World Airlines, Inc.

JAMES H. DOOLITTLE, Sc. D., Vice President, Shell Oil Co.

CARL J. PFINGSTAG, Rear Admiral, United States Navy, Assistant Chief for Field Activities, Bureau of Aeronautics.

DONALD L. PUTT, Lieutenant General, United States Air Force, Deputy Chief of Staff (Development).

DONALD A. QUARLES, D. Eng., Secretary of the Air Force.

ARTHUR E. RAYMOND, Sc. D., Vice President—Engineering, Douglas Aircraft Co., Inc.

FRANCIS W. REICHELDERFER, Sc. D., Chief, United States Weather Bureau.

LOUIS S. ROTHSCHILD, PH. B., Under Secretary of Commerce for Transportation.

NATHAN F. TWINING, General, United States Air Force, Chief of Staff.

HUGH L. DRYDEN, PH. D., *Director*

JOHN W. CROWLEY, JR., B. S., *Associate Director for Research*

JOHN F. VICTORY, LL. D., *Executive Secretary*

EDWARD H. CHAMBERLIN, *Executive Officer*

HENRY J. E. REID, D. Eng., Director, Langley Aeronautical Laboratory, Langley Field, Va.

SMITH J. DEFRANCE, D. Eng., Director, Ames Aeronautical Laboratory, Moffett Field, Calif.

EDWARD R. SHARP, Sc. D., Director, Lewis Flight Propulsion Laboratory, Cleveland, Ohio

WALTER C. WILLIAMS, B. S., Chief, High-Speed Flight Station, Edwards, Calif.

REPORT 1220

CALCULATIONS OF LAMINAR HEAT TRANSFER AROUND CYLINDERS OF ARBITRARY CROSS SECTION AND TRANSPIRATION-COOLED WALLS WITH APPLICATION TO TURBINE BLADE COOLING[1]

By E. R. G. Eckert and J. N. B. Livingood

SUMMARY

An approximate method for the development of flow and thermal boundary layers in the laminar region on cylinders with arbitrary cross section and transpiration-cooled walls is obtained by the use of Karman's integrated momentum equation and an analogous heat-flow equation. Incompressible flow with constant property values throughout the boundary layer is assumed. The velocity and temperature profiles within the boundary layer are approximated by expressions composed of trigonometric functions. Shape parameters for these profiles and functions necessary for the solution of the boundary-layer equations are presented as graphs so that the calculation for any specific case is reduced to the solution of two first-order differential equations.

The method is applied to determine local heat-transfer coefficients and surface temperatures in the laminar flow region of the transpiration-cooled turbine blades for a given coolant flow rate, or to calculate the coolant flow distribution which is necessary in order to keep the blade temperature uniform along the surface.

INTRODUCTION

Transpiration cooling is a very effective means for keeping surfaces that are subject to a hot gas stream at a low temperature. For use of this method, the surface is fabricated from a porous material and a cooling fluid is blown through the pores. Along the outside surface the cooling fluid builds a film that insulates the wall from the hot gas stream. The transpiration-cooling method may be applied to the cooling of structural parts in propulsion systems such as gas-turbine blades, combustion-chamber walls, and rocket nozzles. If a heated fluid is blown through the porous wall, the same method may be used to keep the surface temperature of the wall at a value that is higher than the temperature in the outside flow. In this way, the method may be applied in de-icing of wings or other parts of airplanes and in the propulsion system.

This report presents a method by which the heat transfer connected with transpiration cooling in two-dimensional laminar flow around bodies of arbitrary cross section can be calculated. It considers only the case where the fluid blown through the porous wall is the same as the one in the outside flow. Although the particular application considered in this report is the cooling of turbine blades, the method itself may be applied to other applications as well. The procedure by which the calculation may be carried out for any particular application is described in an appendix of this report.

The determination of the heat transfer is based on the calculation of the thermal boundary layer which builds up around any body in a flow field. This thermal boundary layer is interconnected with the flow boundary layer for variable fluid properties dependent on temperature or superimposed on the velocity boundary layer when the properties are independent of temperature. The build-up of the flow boundary layer is determined by the pressure distribution around the body under consideration. For the type of pressure distribution occurring in the aforementioned applications, only approximate methods of calculation are direct enough for engineering purposes. For the determination of the thermal boundary layer in particular, two types of approach are known.

The first approach was introduced by Kroujiline for the calculation of heat transfer on solid surfaces and presented in more detail by Frösling and others (ref. 1). In this method, the flow boundary layer has to be known before the thermal boundary layer can be calculated.

Usually a method such as that introduced by von Kármán (ref. 2) or Pohlhausen (ref. 3), which fulfills the integrated momentum equation of the boundary layer, is applied for the calculation of the flow boundary layer. More recently, Wieghardt and Walz (ref. 4) have used, in addition to the momentum equation, an integrated energy equation, and Tetervin and Lin (ref. 5) have introduced a still more general integral condition for the boundary layer which may be used in such calculations. The use of these expressions gives better agreement with exact calculations and with measurements in special cases, particularly in regions where the pressure increases in flow direction. Since, in the application considered, the regions of most concern are those where the pressure decreases, the integrated momentum equation, which is simplest to handle, will be used. Schlichting (ref. 6) used this equation to calculate the flow boundary layer on a porous surface through which fluid is sucked in order to keep the boundary layer laminar or to prevent flow separation. A paper by Dorodnitzyn (ref. 7) extended the method to include the effect of Mach number and of variable property values. However, this extension is developed only for zero heat transfer. The calculation of the flow boundary

[1] Supersedes NACA RM E51F22, "Calculations of Laminar Heat Transfer Around Cylinders of Arbitrary Cross Section and Transpiration-Cooled Walls With Application to Turbine Blade Cooling," by E. R. G. Eckert and John N. B. Livingood, 1951.

layer in this report will essentially follow Schlichting's approach.

After the flow boundary layer is determined, the thermal boundary layer can be calculated according to the method of Kroujiline by use of an integrated heat-flow equation. Velocity profiles known from the calculation of the flow boundary layer and temperature profiles within the boundary layer whose shapes are approximated by a polynomial expression are introduced into this heat-flow equation and the equation is solved for the thickness ratio of the thermal boundary layer to the flow boundary layer (ref. 1). This procedure, however, becomes quite lengthy, especially when the number of terms in the polynomial expression for the temperature profile is increased in order to improve the accuracy of the approximation. When an attempt was made at the NACA Lewis laboratory to extend this method, which was previously used only to determine the heat transfer on solid surfaces, to transpiration-cooled porous walls, it was found that the procedure for the solution of the heat-flow equation becomes much simpler and more direct if the equation is solved for a thermal boundary-layer thickness termed convection thickness. This will be explained in detail in a later section of this report. After the method was developed and the calculations were finished, a note by Dienemann (ref. 8) was found in which the same kind of approach is briefly described. Dienemann applies the method to calculate heat-transfer coefficients on solid surfaces and proposes to extend it in such a way as to account for a temperature variation along the solid surface and the influence of internal frictional heating within the boundary layer. He also shows that this method is superior to other approximations which were compared by Goland (ref. 9) with an exact solution for a cylinder with circular cross section. It may be of interest to mention that Goland obtained the exact solution from the fact that the differential equation describing the temperature boundary layer around an infinite cylinder in a flow normal to its axis and for a fluid with a Prandtl number of 1 has exactly the same form as the differential equation describing the spanwise flow within the boundary layer on a yawed infinite cylinder. Calculations of the heat transfer on a transpiration-cooled flat plate which included the variation of property values with temperature were made by Yuan (ref. 10) with the assumption that the total-temperature profile within the boundary layer is similar to the velocity profile. This assumption is valid for a Prandtl number of 1 and for no pressure gradient. The purpose of the present investigation is to consider the influence of pressure gradients as well as Prandtl numbers different from unity.

A second approach for obtaining an approximate solution of the thermal boundary layer was described in reference 1. It is still simpler than the approach by Kroujiline, since in this method it is not necessary to calculate the flow boundary layer prior to the determination of the thermal boundary layer. This method uses exact solutions of the boundary-layer equations which are known for a special type of pressure variation in the flow which is encountered on wedge-shaped bodies. These velocity profiles and the temperature profiles are used to approximate the actual profiles for arbitrary pressure variations. A differential equation is set up with the condition that the growth of the boundary layer at any place on the cylinder with arbitrary cross section be the same as for the wedge-type flow when the boundary-layer thickness and the pressure gradient have the same values in both cases. When this idea is applied to the momentum thickness of the boundary layer, the resulting equation is identical with Kármán's integrated momentum equation. When it is applied to the convection thickness of the thermal boundary layer, the resulting differential equation fulfills the requirement that the heat transferred from the surface to the fluid must be found again within the boundary layer (ref. 11). This method was compared with exact solutions and experimental values in reference 1 and in investigations performed at the University of California (ref. 12), and the agreement obtained was quite satisfactory. This method can easily be extended to include effects of variations of the surface temperature and of internal heating (ref. 11); however, the corresponding exact solutions for the wedge-type flow must be known. Such solutions, which take into account the effects of a surface temperature variation and of internal heating, are presented in references 11 and 13. The method may also be extended to the transpiration cooling of porous surfaces as soon as the corresponding exact solutions for this case are known. A few of these solutions are presented in reference 14. However, too few solutions are given for use as a basis for the approximate method. Brown (ref. 15) has recently made an extensive calculation to obtain exact solutions in transpiration-cooled porous surfaces of the wedge-flow type which include the effect of pressure gradients and of variable property values. The results of this calculation are now being used to extend the method mentioned in the preceding paragraph to transpiration cooling.

This paper deals with the method described as the first type of approach. The method has the advantage of being applicable to cases for which the corresponding wedge-type flow and heat transfer are not known.

STATEMENT OF PROBLEM AND SIMPLIFYING ASSUMPTIONS

This report is a contribution to the problem of determining the development of the thermal boundary layer and the heat-transfer coefficients on a body of arbitrary cross section with porous walls in a two-dimensional flow. Figure 1 shows the cross section of a body of this type. At Reynolds numbers that are sufficiently high, the flow around the body may be subdivided into the boundary-layer region, which surrounds the body with a very small thickness, and the

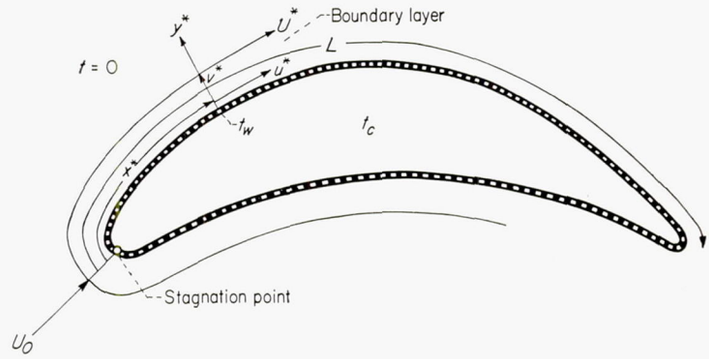

FIGURE 1.—Sketch of turbine blade indicating notations used.

potential flow, which determines the pressure distribution around the body. The highest pressure on the body is found at the stagnation point. The pressure then decreases in flow direction along both sides of the body and usually increases again later. The pressure variation along the body determines the development of the flow boundary layer and also whether the boundary layer is laminar or turbulent. Usually, the laminar part is confined to a region near the nose of the body. The laminar boundary-layer region is investigated herein. The flow of coolant through the porous surface may be described by the velocity v_w with which the coolant leaves the surface in a normal direction. The questions which will be answered in this report are (1) what are the local heat-transfer coefficient and the surface temperature on any point along the body for any prescribed distribution of the coolant velocity, and (2) what distribution of the coolant velocity gives a desired distribution of the heat-transfer coefficient and of the surface temperature around the body. Usually, for example, a constant wall temperature is most desirable and the problem is to determine that distribution of the coolant velocity which results in a constant wall temperature.

A number of simplifications must be introduced in order to keep the time required for the solution of a special problem within a tolerable amount. The following assumptions are made: The flow is two-dimensional and in steady state, internal frictional heating within the boundary layer can be neglected, and property values (density, viscosity, and heat conductivity) may be considered constant. The influence of temperature gradients along the surface of the body is neglected. Although this influence may be considerable (ref. 13), there is no quantitative information available for transpiration-cooled surfaces that would permit this effect to be taken into account.

In applying the method to the determination of the temperatures of transpiration-cooled turbine blades, neglecting internal frictional heating should be admissible, since the temperature differences within the boundary layer generated by the cooling process are considerably larger than those generated by aerodynamic heating. This will be shown in more detail later. On the other hand, the large temperature variation in the boundary layer is connected with a considerable variation of the property values. The influence of this variation on the heat transfer may be approximately corrected by use of the results in reference 15.

BOUNDARY-LAYER EQUATIONS

In a coordinate system, shown in figure 1, where the x-axis runs along the surface and the y-direction is normal to the surface and under the assumptions mentioned in the previous section, the differential equations describing the velocity and the temperature within the boundary layer are

$$\rho u^*\frac{\partial u^*}{\partial x^*}+\rho v^*\frac{\partial u^*}{\partial y^*}=-\frac{\partial p^*}{\partial x^*}+\mu\frac{\partial^2 u^*}{\partial y^{*2}} \tag{1}$$

$$\frac{\partial u^*}{\partial x^*}+\frac{\partial v^*}{\partial y^*}=0 \tag{2}$$

$$\rho c_p u^*\frac{\partial t}{\partial x^*}+\rho c_p v^*\frac{\partial t}{\partial y^*}=k\frac{\partial^2 t}{\partial y^{*2}} \tag{3}$$

(All symbols are defined in appendix A.) The equations have to fulfill the following boundary conditions: At the surface ($y=0$), the velocity component u^* parallel to the surface is 0, the velocity component v^* normal to the surface has a finite value $v_w{}^*$, and the temperature of the surface is interconnected with the velocity $v_w{}^*$ by the over-all heat-transfer process, so that only one of the two values may be prescribed. At the outer edge of the boundary layer ($y=\infty$), the u^* component of the velocity transforms asymptotically into the stream volocity U^* and the temperature transforms into the stream temperature. Since only temperature differences appear in equation (3), the temperature level does not enter into the problem. Therefore, all temperatures will be measured from the temperature in the stream as reference temperature, and t will be interpreted as the temperature difference from this reference temperature. Consequently, outside of the boundary layer, $t=0$.

In a gas stream, it is advantageous to interpret t as the total temperature difference. In this case, equation (3) already includes the effect of the frictional heating for a gas with a Prandtl number of 1. Since for all gases, the Prandtl number does not deviate much from the value 1, equation (3) also gives a good approximation to the real conditions for gases as long as the temperature differences impressed upon the boundary layer by a cooling process are larger than the temperature differences created by internal friction.

In order to reduce the number of parameters, the differential equations will be made dimensionless. For this purpose, all lengths measured parallel to x are divided by L, the distance between the stagnation point and the trailing edge of the body measured along the surface, and all velocities in this direction are divided by an upstream velocity U_0. All lengths and all velocities parallel to y are, in addition, multiplied by the square root of Reynolds numbers Re_0 based on the body length L and the upstream velocity U_0:

$$x=\frac{x^*}{L} \quad u=\frac{u^*}{U_0} \quad y=\frac{y^*}{L}\sqrt{Re_0} \quad v=\frac{v^*}{U_0}\sqrt{Re_0} \tag{4}$$

The pressure gradient $\partial p^*/\partial x^*$ is impressed upon the boundary layer by the potential flow outside the boundary layer and can be replaced by the stream velocity gradient by use of Bernoulli's equation:

$$-\frac{\partial p^*}{\partial x^*}=\rho U^*\frac{\partial U^*}{\partial x^*} \tag{5}$$

In this way, equations (1) to (3) transform into

$$u\frac{\partial u}{\partial x}+v\frac{\partial u}{\partial y}=U\frac{\partial U}{\partial x}+\frac{\partial^2 u}{\partial y^2} \tag{6}$$

$$\frac{\partial u}{\partial x}+\frac{\partial v}{\partial y}=0 \tag{7}$$

$$u\frac{\partial t}{\partial x}+v\frac{\partial t}{\partial y}=\frac{1}{Pr}\frac{\partial^2 t}{\partial y^2} \tag{8}$$

The boundary conditions for these equations become

$$y=0 \qquad u=0 \qquad v=v_w(x) \qquad t=t_w(x) \tag{9}$$

$$y\rightarrow\infty \qquad u\rightarrow U \qquad t\rightarrow 0 \tag{10}$$

The equations are now integrated over y from $y=0$ to $y=\infty$. The result of this integration is Kármán's integrated momentum equation

$$\frac{d}{dx}\int_0^\infty (U-u)u\,dy+\frac{dU}{dx}\int_0^\infty (U-u)\,dy-v_wU=\left(\frac{\partial u}{\partial y}\right)_w \tag{11}$$

and the heat-flow equation

$$\frac{d}{dx}\int_0^\infty tu\,dy-t_wv_w=-\frac{1}{Pr}\left(\frac{\partial t}{\partial y}\right)_w \tag{12}$$

In order to simplify these equations, the following characteristic boundary-layer thicknesses are introduced:

(1) The displacement thickness of the flow boundary layer

$$\delta_d=\int_0^\infty\left(1-\frac{u}{U}\right)dy \tag{13}$$

(2) The momentum or impulse thickness of the flow boundary layer

$$\delta_i=\int_0^\infty \frac{u}{U}\left(1-\frac{u}{U}\right)dy \tag{14}$$

(3) The convection thickness of the thermal boundary layer

$$\delta_{t,c}=\int_0^\infty \theta\frac{u}{U}\,dy \tag{15}$$

where θ is the ratio t/t_w with the limiting values $\theta=1$ for $y=0$ and $\theta=0$ for $y=\infty$. Introducing these boundary-layer thicknesses and writing dU/dx as U' transforms equations (11) and (12) into

$$\frac{d}{dx}(U^2\delta_i)+\delta_dUU'-v_wU=\left(\frac{\partial u}{\partial y}\right)_w \tag{16}$$

$$\frac{d}{dx}(t_wU\delta_{t,c})-t_wv_w=-\frac{t_w}{Pr}\left(\frac{\partial\theta}{\partial y}\right)_w \tag{17}$$

VELOCITY AND TEMPERATURE PROFILES

In order to obtain an approximate solution of the last two equations, approximate expressions for the velocity and temperature profiles will be introduced. The accuracy of the results of this calculation will depend on how well the actual profiles are approximated by the assumed shapes. The temperature profiles as well as the velocity profiles are chosen as a one-parameter family. The parameter for each family is determined in such a way that the assumed profiles fulfill the exact boundary-layer equations (6) to (8) at the wall surface:

$$v_w\left(\frac{\partial u}{\partial y}\right)_w=U\frac{\partial U}{\partial x}+\left(\frac{\partial^2 u}{\partial y^2}\right)_w \tag{18}$$

$$v_w\left(\frac{\partial\theta}{\partial y}\right)_w=\frac{1}{Pr}\left(\frac{\partial^2\theta}{\partial y^2}\right)_w \tag{19}$$

In addition, the following boundary conditions will be fulfilled:

$$y=0 \quad u=0 \quad \theta=1 \tag{20}$$

$$y\to\infty \quad u\to U \quad \theta\to 0 \tag{21}$$

Originally, polynomial expressions were used to approximate both the velocity and the temperature profiles. Schlichting, however, pointed out that better approximations may be obtained by expressions composed of trigonometric functions (ref. 6). The following profiles are used in this report:

Velocity profile.—For $\Delta\geq 0$, $0\leq\frac{y}{\delta}\leq 1$,

$$\left.\begin{aligned}&\frac{u}{U}=\sin\frac{\pi}{2}\frac{y}{\delta}+\Delta\left(1-e^{-3\frac{y}{\delta}}-\sin\frac{\pi}{2}\frac{y}{\delta}\right)\\ &\text{and for } \frac{y}{\delta}\geq 1,\\ &\frac{u}{U}=1-\Delta e^{-3\frac{y}{\delta}}\end{aligned}\right\} \tag{22}$$

By use of this profile, the following expression is found from equation (18) for the shape parameter Δ:

$$\Delta=\frac{U'\delta^2-\frac{\pi}{2}v_w\delta}{9+\left(3-\frac{\pi}{2}\right)v_w\delta} \tag{23}$$

The velocity profile equation (22) has already been used by Schlichting (ref. 6). For a solid flat plate ($U'=0$ and $v_w=0$), it approximates the Blasius velocity profile very well, and for $U'=0$ and $v_w=-3/\delta$, transforms into the exact asymptotic suction profile as calculated by Schlichting (ref. 6).

For $\Delta\leq 0$, $0\leq\frac{y}{\delta}\leq 1$,

$$\left.\begin{aligned}&\frac{u}{U}=\sin\frac{\pi}{2}\frac{y}{\delta}+\Delta\sin\frac{\pi}{2}\frac{y}{\delta}\left(1-\sin\frac{\pi}{2}\frac{y}{\delta}\right)\\ &\text{and for } \frac{y}{\delta}\geq 1,\\ &\frac{u}{U}=1\end{aligned}\right\} \tag{24}$$

The shape parameter in this case, as obtained from equation (18), is

$$\Delta=\frac{U'\delta^2-\frac{\pi}{2}v_w\delta}{\frac{\pi^2}{2}+\frac{\pi}{2}v_w\delta} \tag{25}$$

For the solid flat plate, this profile gives the same expression as equation (22). It will be shown later that the profile approximates the separation profile as calculated by Hartree (ref. 16) better than the usual polynomial expression. Separation occurs at $\Delta=-1$ and the corresponding profile has the shape

$$\frac{u}{U}=\sin^2\frac{\pi}{2}\frac{y}{\delta} \tag{26}$$

Temperature profile.—For $0\leq\frac{y}{\delta_t}\leq 1$,

$$\left.\begin{aligned}&\frac{t}{t_w}=\theta=1-\sin\frac{\pi}{2}\frac{y}{\delta_t}-\Delta_t\sin\frac{\pi}{2}\frac{y}{\delta_t}\left(1-\sin\frac{\pi}{2}\frac{y}{\delta_t}\right)\\ &\text{and for } \frac{y}{\delta_t}\geq 1,\\ &\theta=0\end{aligned}\right\} \tag{27}$$

The shape factor for this profile is obtained from equation (19) as follows:

$$\Delta_t=\frac{-Pr\,v_w\delta_t}{\pi+Pr\,v_w\delta_t} \tag{28}$$

In this case, a negative shape factor Δ_t is always connected with a positive value of v_w, whereas for the velocity profile, the sign of the shape factor depends, in addition, on the pressure gradient dU/dx.

With these profiles, the different boundary-layer thicknesses and the velocity gradient at the wall may be calculated.

$$\left.\begin{aligned}
&\frac{\delta_d}{\delta}=\left(1-\frac{2}{\pi}\right)-\left(\frac{2}{3}-\frac{2}{\pi}\right)\Delta && (29)\\
&\frac{\delta_i}{\delta}=0.1366+0.03791\,\Delta-0.00786\,\Delta^2 && (30)\\
&\left(\frac{du}{dy}\right)_w=\frac{U}{\delta}\left[\frac{\pi}{2}+\left(3-\frac{\pi}{2}\right)\Delta\right] && (31)
\end{aligned}\right\}\Delta>0$$

$$\left.\begin{aligned}
&\frac{\delta_d}{\delta}=\left(1-\frac{2}{\pi}\right)-\left(\frac{2}{\pi}-\frac{1}{2}\right)\Delta && (32)\\
&\frac{\delta_i}{\delta}=0.1366-0.01456\Delta-0.02618\,\Delta^2 && (33)\\
&\left(\frac{du}{dy}\right)_w=\frac{\pi}{2}\frac{U}{\delta}(1+\Delta) && (34)
\end{aligned}\right\}\Delta<0$$

The nondimensional temperature gradient at the wall is

$$\left(\frac{d\theta}{dy}\right)_w=-\frac{\pi}{2}\frac{1}{\delta_t}(1+\Delta_t) \tag{35}$$

The corresponding expressions for the convection thickness of the thermal boundary layer are presented in appendix B.

TRANSFORMATION OF BOUNDARY-LAYER EQUATIONS

FLOW BOUNDARY LAYER

Multiplication of equation (16) by δ_i/U and a partial differentiation of the first term give

$$U\delta_i\frac{d\delta_i}{dx}+\left(2+\frac{\delta_d}{\delta_i}\right)U'\delta_i^2-v_w\delta_i=\frac{\delta_i}{U}\left(\frac{\partial u}{\partial y}\right)_w \tag{36}$$

The expression in the parentheses of the second term on the left-hand side and the term on the right-hand side are functions of the shape parameter Δ. Therefore, the momentum equation for the boundary layer may be written in its final form.

$$\frac{U}{2}\frac{d(\delta_i^2)}{dx}=f_2(\Delta)-f_1(\Delta)U'\delta_i^2+v_w\delta_i \tag{37}$$

with the following expressions for the two functions f_1 and f_2, which are obtained from equations (29) to (34):

$$\left.\begin{aligned}
&f_1(\Delta)=2+\frac{0.3634-0.03005\Delta}{0.1366+0.03791\,\Delta-0.00786\Delta^2} && (38)\\
&f_2(\Delta)=\left[\frac{\pi}{2}+\left(3-\frac{\pi}{2}\right)\Delta\right](0.1366+0.03791\Delta-0.00786\Delta^2 && (39)
\end{aligned}\right\}\Delta\geq 0$$

$$\left.\begin{aligned}
&f_1(\Delta)=2+\frac{0.3634-0.1366\Delta}{0.1366-0.01456\Delta-0.02618\Delta^2} && (40)\\
&f_2(\Delta)=\frac{\pi}{2}(1+\Delta)\,(0.1366-0.01456\Delta-0.02618\Delta^2 && (41)
\end{aligned}\right\}\Delta\leq 0$$

These functions are presented in figure 2. All curves have a break at $\Delta=0$ because different expressions approximate the velocity profiles for positive and negative Δ values. Equation (37) is a linear first-order differential equation from which the momentum thickness of the boundary layer

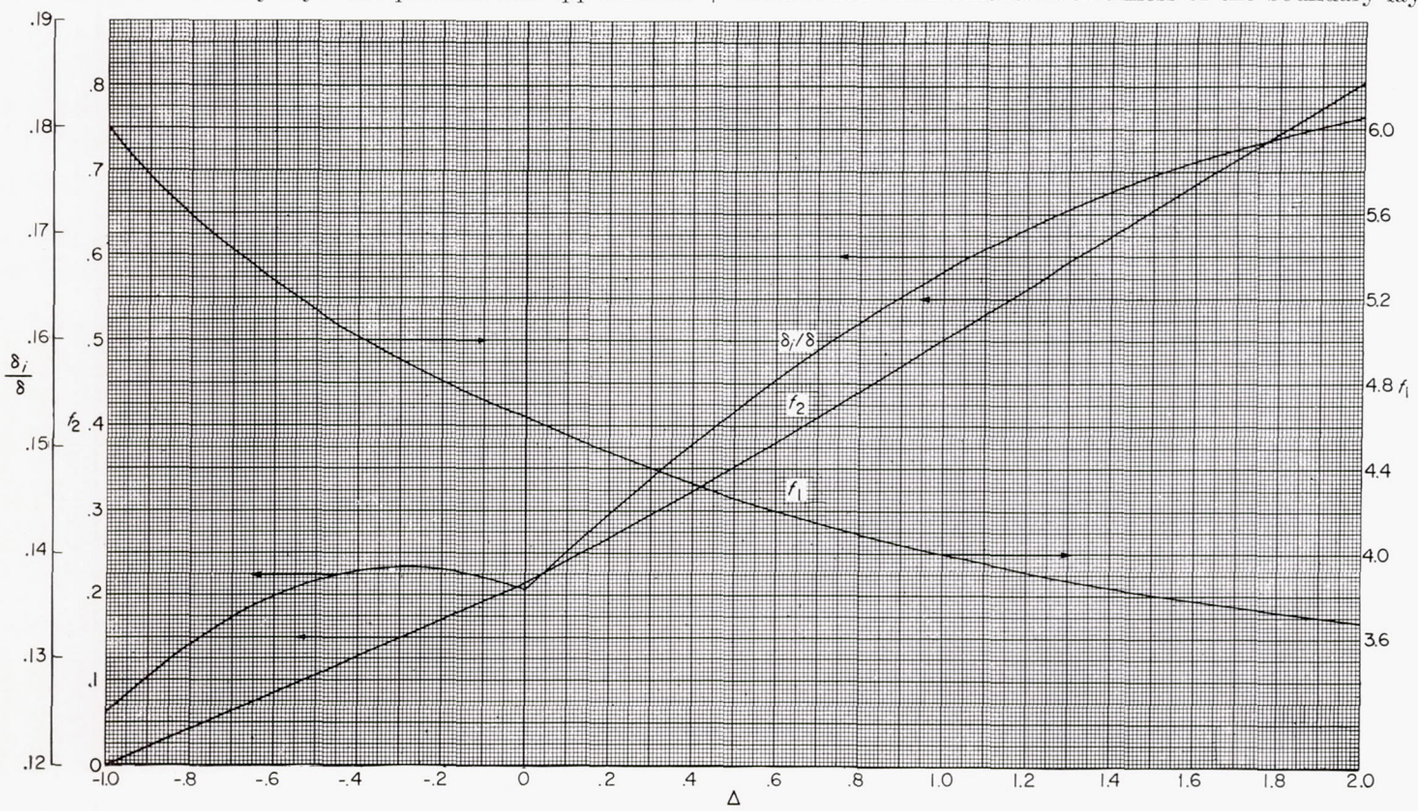

FIGURE 2.—Chart for determination of f_1, f_2, and δ_i/δ used in flow boundary-layer differential equation. (An 18- by 10½-in. working chart of this figure may be obtained upon request from NACA Headquarters.)

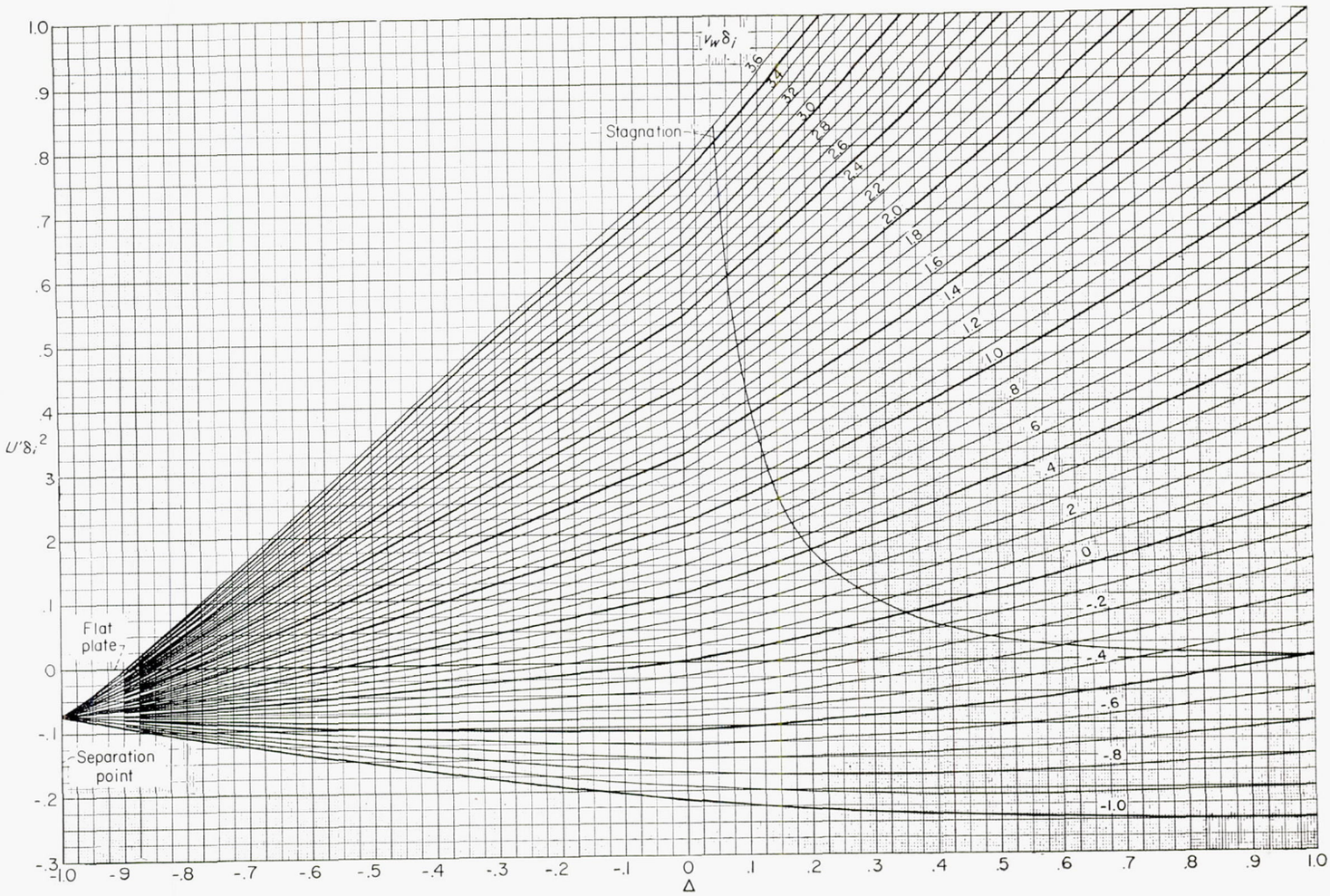

FIGURE 3.—Chart for determination of shape parameter Δ for flow boundary-layer calculations. (A 22- by 15½-in. working chart of this figure may be obtained upon request from NACA Headquarters.)

can be obtained by integration, as soon as the gradient U' of the stream velocity U and the porous flow characterized by v_w are known as functions of x. In order to make the calculations more convenient, the shape parameter Δ can be expressed as a function of the two quantities $U'\delta_i^2$ and $v_w\delta_i$

$$\Delta \geq 0, \Delta = \frac{U'\delta_i^2 - \frac{\pi}{2} v_w\delta_i \frac{\delta_i}{\delta}}{9\left(\frac{\delta_i}{\delta}\right)^2 + \left(3 - \frac{\pi}{2}\right) v_w\delta_i \frac{\delta_i}{\delta}} \tag{42}$$

$$\Delta \leq 0, \Delta = \frac{U'\delta_i^2 - \frac{\pi}{2} v_w\delta_i \frac{\delta_i}{\delta}}{\frac{\pi^2}{2}\left(\frac{\delta_i}{\delta}\right)^2 + \frac{\pi}{2} v_w\delta_i \frac{\delta_i}{\delta}} \tag{43}$$

The ratio δ_i/δ occurring in these equations is a function of Δ (see eqs. (30) and (33) and fig. 2). The functional relation for Δ is plotted in figure 3. By use of figures 2 and 3, the integration procedure for the differential equation (37) becomes very simple. The step-by-step procedure for such a calculation is presented in appendix C.

In order to start the calculation at the stagnation point, the boundary-layer thickness δ_i at this location must be known. At the stagnation point, the stream velocity U is zero. Since, on a blunt nose, the increase of the boundary-layer thickness is never infinite, the term on the right-hand side of equation (37) has to be zero. This gives the equation

$$f_2(\Delta) - f_1(\Delta) U'\delta_i^2 + v_w\delta_i = 0 \tag{44}$$

However, figure 3 also applies to the conditions at the stagnation point. From both relations, $U'\delta_i^2$, Δ, f_1, and f_2 were

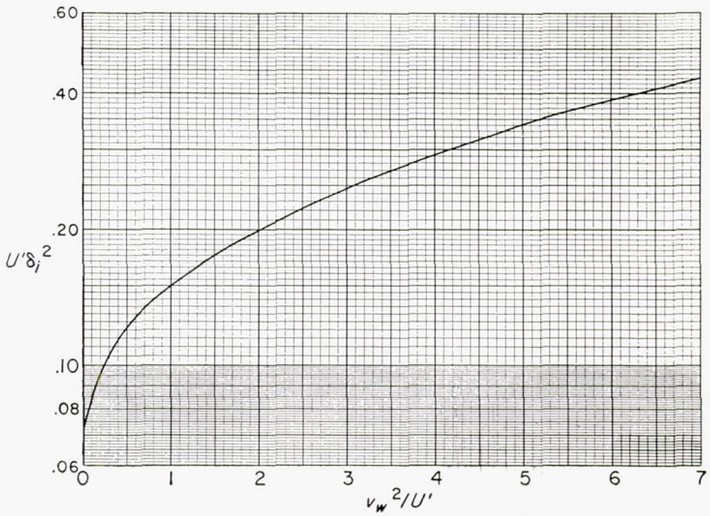

FIGURE 4.—Chart for determination of $U'\delta_i^2$ at stagnation point for flow boundary-layer calculations.

each obtained as a function of $v_w\delta_i$ by a trial-and-error process. These values are presented in table I. The connection between $U'\delta_i^2$, Δ, and $v_w\delta_i$ is also shown in figure 3 as the stagnation line. Table I cannot be used immediately to start the calculation because the value $v_w\delta_i$ is not known. However, the value $\frac{(v_w\delta_i)^2}{U'\delta_i^2}=\frac{v_w^2}{U'}$, which contains only known values, is also a function of $U'\delta_i^2$ and is plotted in figure 4. From this figure, $U'\delta_i^2$ can be determined for a given v_w^2/U' and δ_i can then be obtained from this value.

THERMAL BOUNDARY LAYER

With the help of equations (28) and (35), the heat-flow equation (17) is transformed into

$$\frac{1}{v_w}\frac{d}{dx}(U\delta_{t,c})=1+\frac{\pi}{2}\frac{1}{PrKv_w\delta}\left(1-\frac{PrKv_w\delta}{\pi+PrKv_w\delta}\right)-\frac{U\delta_{t,c}}{v_wt_w}\frac{dt_w}{dx} \tag{45}$$

where K denotes the ratio δ_t/δ. The last term on the right-hand side accounts for a variation of the temperature along the surface. A difficulty arises in connection with this term. It is known from the results of references 11 and 13 that a temperature gradient dt_w/dx also has a pronounced effect on the shape of the temperature profile. Since no such effect was included in the assumed profile (eq. (27)), the significance of the last term is doubtful. It was therefore neglected herein, restricting this report to cases where the variation of the surface temperature is kept small either by internal conduction within the wall or by proper choice of v_w. The investigation of the influence of large surface temperature gradients will be left to future work. With this simplification, equation (45) can be written in its final form

$$\frac{d}{dx}(U\delta_{t,c})=v_wf_3(PrKv_w\delta) \tag{46}$$

where f_3 is a function of the product $Pr\ Kv_w\delta$, as presented in figure 5. For a solid wall ($v_w=0$), the equation simplifies to

$$\frac{d}{dx}(U\delta_{t,c})=\frac{\pi}{2}\frac{1}{KPr\delta} \tag{47}$$

The shape parameter Δ_t may be written in the form

$$\Delta_t=\frac{-Pr\ Kv_w\delta}{\pi+Pr\ Kv_w\delta} \tag{48}$$

This equation, together with the expressions for $\delta_{t,c}/\delta$ (appendix B), determines a functional relation between K, $\delta_{t,c}/\delta$, Δ, and $Pr\ v_w\delta$, which is presented in figure 6. The figure presents the ratios $\delta_{t,c}/\delta$ for each of three values of the shape parameter Δ (-1, 0, and $+1$). For intermediate values of Δ, linear interpolation in the range $\Delta=-1$ to $\Delta=0$, or $\Delta=0$ to $\Delta=1$, at a constant value of K may be used with good accuracy. The heat-flow equation (46) is again a linear first-order differential equation from which the thermal convection thickness is obtained by integration when the stream velocity U, the flow through the porous surface v_w, and the Prandtl number Pr are prescribed, and the boundary layer thickness δ and the shape factor of the flow boundary layer Δ are known from a preceding solution of equation (37). The step-by-step procedure for such a calculation is explained in appendix C.

In order to start the calculation, the convection thickness $\delta_{t,c}$ must be known at the stagnation point. A partial differentiation of the left-hand side of equation (46) gives

$$U\frac{d\delta_{t,c}}{dx}+U'\delta_{t,c}=v_wf_3$$

At the stagnation point, U is zero, and the boundary-layer increase $d\delta_{t,c}/dx$ is not infinite on a blunt-nosed body. This results in the equation

$$\frac{U'}{v_w}\delta_{t,c}=f_3(Pr\ Kv_w\delta)$$

or

$$\frac{U'\delta^2}{v_w\delta}\frac{\delta_{t,c}}{\delta}=f_3(Pr\ Kv_w\delta) \tag{49}$$

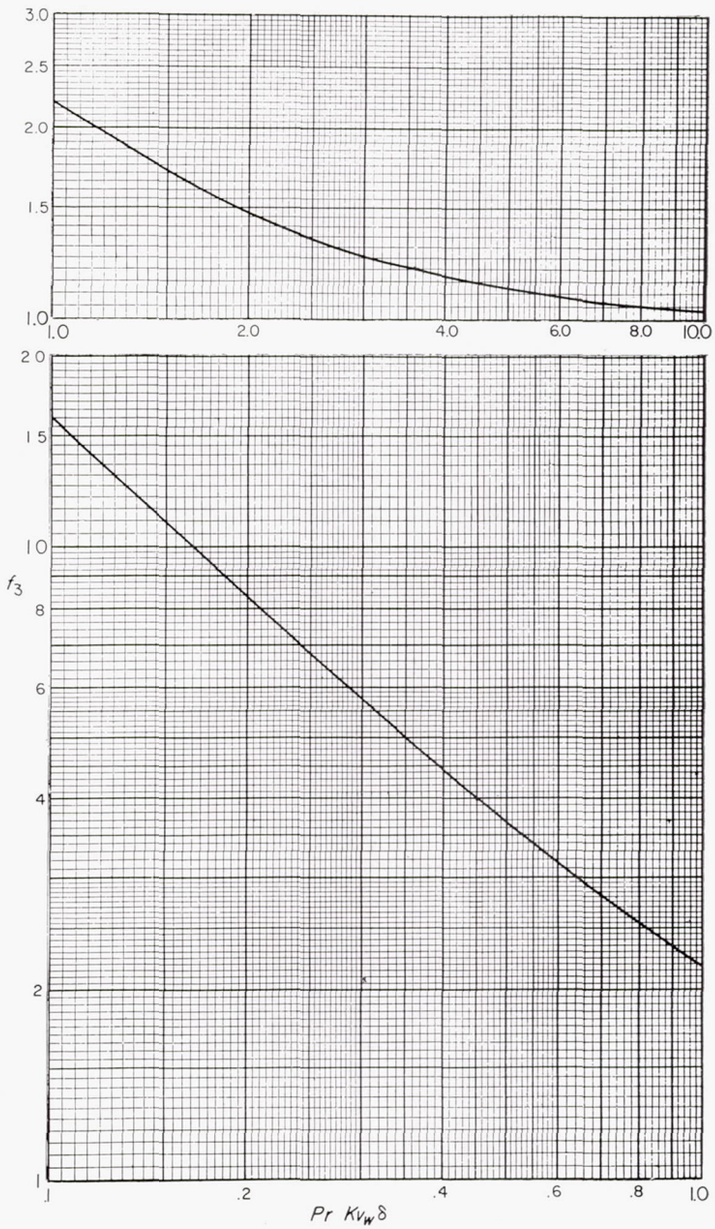

FIGURE 5.—Chart for determination of f_3 used in thermal boundary-layer differential equation.

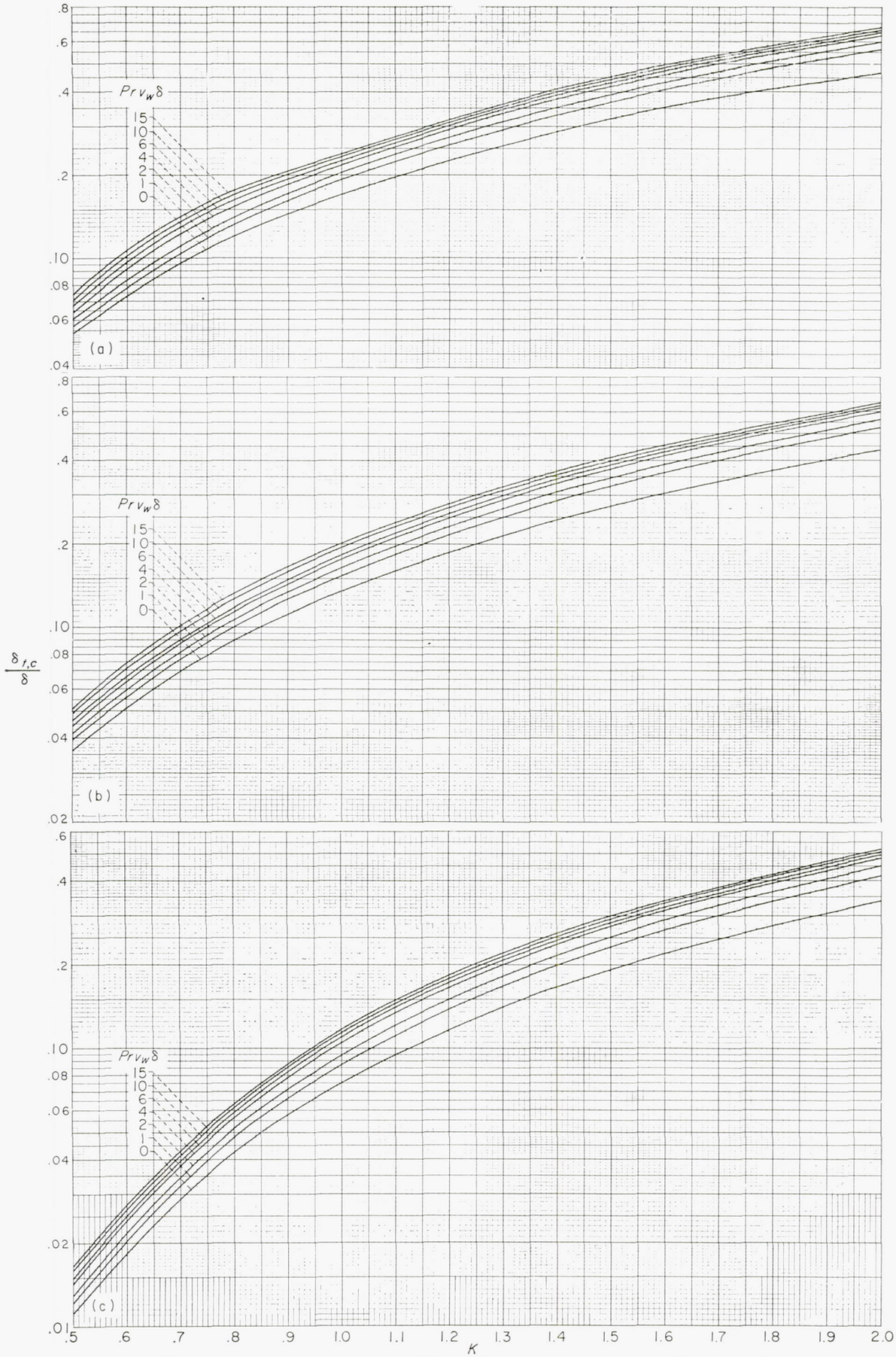

(a) $\Delta = 1$. (b) $\Delta = 0$. (c) $\Delta = -1$.

FIGURE 6.—Chart for determination of K for thermal boundary-layer calculations. (A 17- by 20-in. working chart of this figure may be obtained upon request from NACA Headquarters.)

This is a relation between the two unknown ratios $\delta_{t,c}/\delta$ and K. A second relation is given by figure 6. From both, the values $\delta_{t,c}/\delta$ and K can be determined by a trial-and-error procedure. The values are presented in table II and figure 7.

When the thermal convection boundary-layer thickness is known, the local heat-transfer coefficient follows by a simple calculation. The equation which defines the local heat-transfer coefficient h is

$$ht_w=-k\left(\frac{\partial t}{\partial y^*}\right)_w \tag{50}$$

This equation gives, for the local Nusselt number based on the length L,

$$Nu=\frac{hL}{k}=-\frac{L}{t_w}\left(\frac{\partial t}{\partial y^*}\right)_w=-\sqrt{Re_0}\left(\frac{\partial \theta}{\partial y}\right)_w \tag{51}$$

The introduction of equation (17) for the temperature gradient leads to the expression

$$\frac{Nu}{\sqrt{Re_0}}=Pr\left[\frac{1}{t_w}\frac{d}{dx}(t_wU\delta_{t,c})-v_w\right]=v_w\,Pr\,(f_3-1) \tag{52}$$

Without porous cooling, equation (52) simplifies to

$$\frac{Nu}{\sqrt{Re_0}}=\frac{\pi}{2}\frac{1}{K\delta} \tag{53}$$

In many cases, all the heat transferred from the outside flow to the wall surface is picked up by the cooling fluid on its flow through the porous wall. In this case, the wall surface temperature may be calculated by the equation

$$ht_w=\rho c_p v_w^*\,(t_c-t_w) \tag{54}$$

where t_c is the temperature with which the coolant enters the porous wall. The ratio of the difference in gas temperature minus wall surface temperature to the difference in gas temperature minus coolant temperature is given by the expression

$$\Phi=\frac{t_w}{t_c}=\frac{1}{1+\dfrac{h}{\rho c_p v_w^*}}=\frac{1}{f_3} \tag{55}$$

COMPARISON OF ASSUMED VELOCITY AND TEMPERATURE PROFILES WITH EXACT SOLUTIONS

The accuracy of the method depends on how well the assumed profiles approximate the actual ones. It is therefore necessary to check the accuracy of this approximation with the results of exact calculations to the extent that these are available. Such a comparison will be made in this section.

VELOCITY PROFILES

For the solid surface ($v_w=0$), the comparison can be made with exact solutions, which were obtained by Hartree (ref. 16), for wedge-type flow for which the stream velocity is a power function of the distance from the stagnation point ($U=U_1x^m$). A set of velocity profiles taken from reference 16 is presented as a family of dashed lines in figure 8, where the ratio of the velocity u in the boundary layer to the stream velocity U outside of the boundary layer is plotted over the dimensionless distance

$$z=\frac{y^*}{\sqrt{2-\beta}}\sqrt{\frac{U^*}{\nu x^*}}=\frac{y}{\sqrt{2-\beta}}\sqrt{\frac{U}{x}}$$

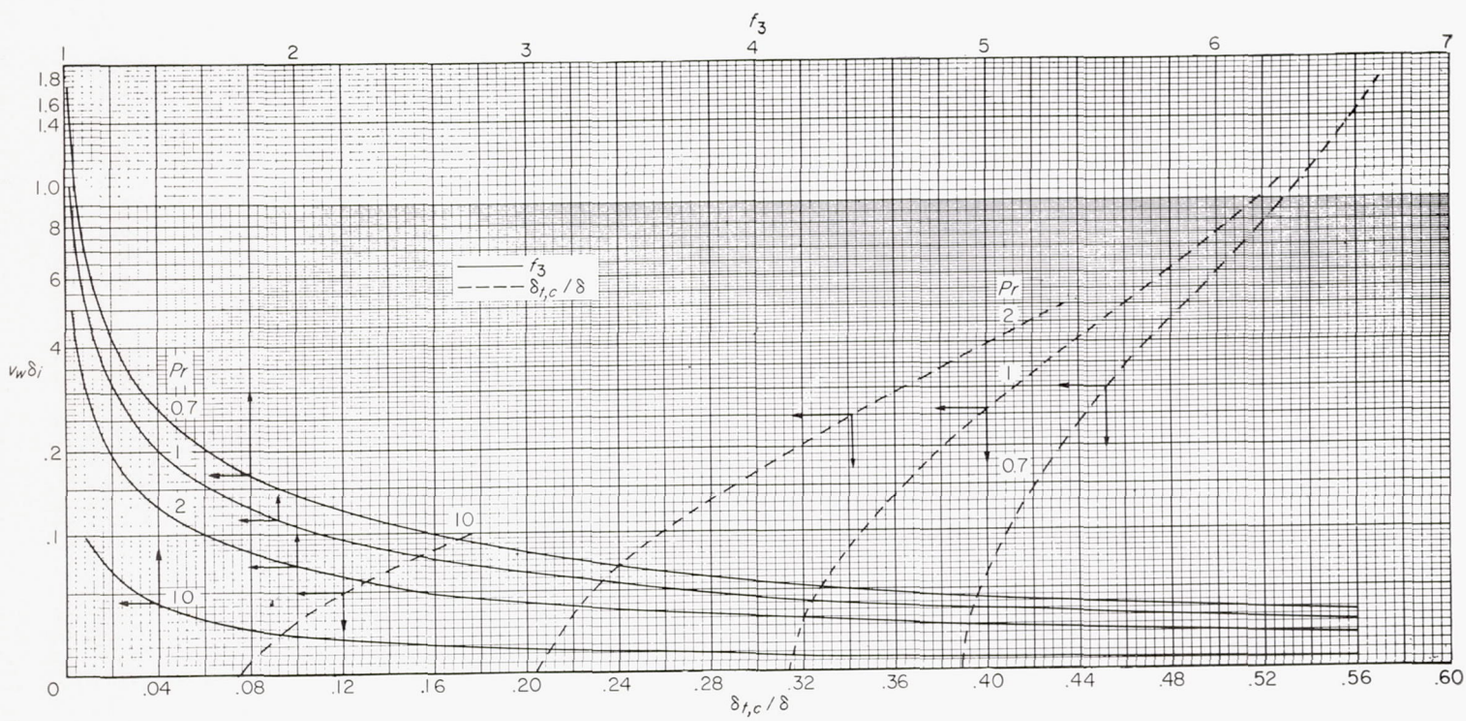

FIGURE 7.—Chart for determination of $\delta_{t,c}/\delta$ and f_3 at stagnation point for thermal boundary-layer calculations. (A 17- by 9-in. working chart of this figure may be obtained upon request from NACA Headquarters.)

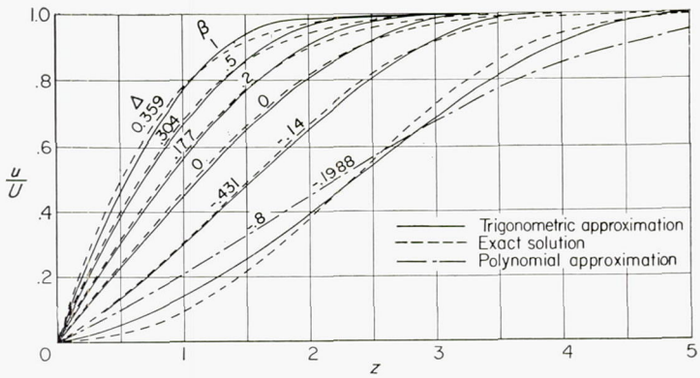

FIGURE 8.—Comparison of approximate velocity profiles for solid surface with Hartree solutions (ref. 16). v_w, 0.

and the shape parameter β is defined by the equation $\beta=\frac{2m}{m+1}$. The expression for the dimensionless displacement thickness is $z_i=\frac{\delta}{\sqrt{2-\beta}}\sqrt{\frac{U}{x}}$. Therefore,

$$\beta z_i^2=\frac{\beta}{2-\beta}\,\delta_i^2\,\frac{U}{x}$$

A differentiation of $U=U_1x^m$ gives $U'=m\,\frac{U}{x}=\frac{\beta}{2-\beta}\,\frac{U}{x}$. Therefore,

$$\beta z_i^2=U'\delta_i^2 \tag{56}$$

The value z_i as a function of β is presented in reference 1. Since $U'\delta_i^2$ is a function of Δ, according to equations (42) and (43), equation (56) presents a relation between β and Δ from which Δ may be calculated for any value of β. The shape of the approximate velocity profile is determined by Δ (eqs. (22) and (24)). In this way, the solid profiles of figure 8 were determined. They are superimposed on the exact profiles in such a way that the displacement thickness is the same in both cases. Figure 8 shows that generally the agreement between the exact profiles and the approximation used in this report is satisfactory. Only for the separation profile ($\beta=-0.1988$) are the deviations larger, but even for this separation profile the approximation by equation (24) is better than the usual four-term polynomial approximation, which is shown as a dash-dot line.

For a porous wall, some exact solutions are contained in reference 14. The notations in this reference are the same as the ones mentioned in the previous paragraph in connection with the Hartree solutions. In that report the porous flow velocity v_w is characterized by

$$\lambda=v_w\sqrt{\frac{x^*}{\nu U^*}}=v_w\sqrt{\frac{x}{U}}$$

From this and the previous expression for z_i

$$\sqrt{2-\beta}\;\lambda\;z_i=v_w\delta_i \tag{57}$$

The value of z_i is presented in reference 14 as a function of λ for two values of β (0 and 1). Therefore, equation (57) presents a relation between λ and Δ for a certain value of β. Equation (57) therefore connects the parameter λ, which determines the shape of the exact velocity profile, with the

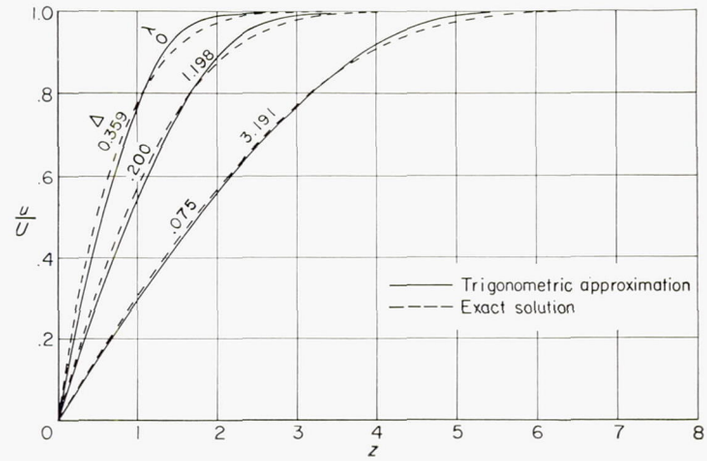

FIGURE 9.—Comparison of approximate velocity profiles near stagnation point with Schlichting solutions (ref. 14). β, 1.

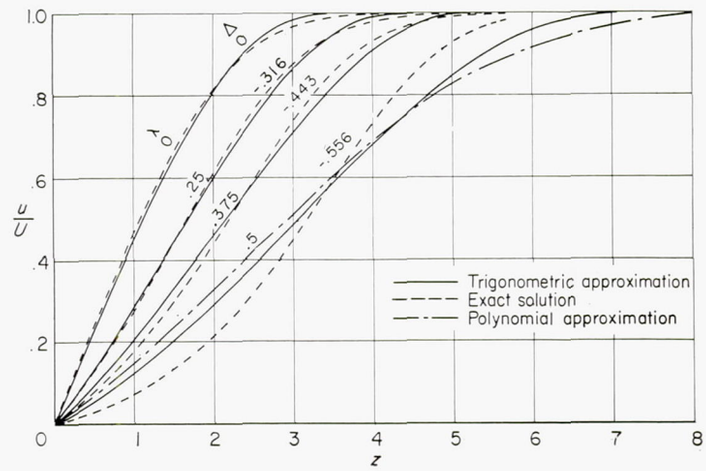

FIGURE 10.—Comparison of approximate velocity profiles for flat plate with Schlichting solutions (ref. 14). β, 0.

form parameter Δ determining the shape of the approximation. Figures 9 and 10 show a comparison between the exact profiles and the approximations for the neighborhood of the stagnation point ($\beta=1$) and for a flat plate ($\beta=0$). It may be seen that again this agreement is quite satisfactory for $\beta=1$. For $\beta=0$ the approximation is not as good for profiles with a distinct S shape. For the largest coolant flow (characterized by the highest value of λ or the smallest value of Δ) the deviation is considerable, although the agreement is somewhat better than that with the four-term polynomial approximation indicated by a dash-dot line. Therefore, the method presented in this report should not be used for excessive coolant-flow rates.

TEMPERATURE PROFILE

For a solid wall ($v_w=0$), the approximate expression (eq. (27)) for the temperature profile has a unique form, independent of the pressure gradient along the surface. For a gas with a Prandtl number of 1 and constant pressure along the surface, it is known that the temperature profile is similar to the Blasius velocity profile. This similarity also holds for the approximation in this report. In addition, it is shown in reference 1 that the shape of the actual temperature profile is influenced only to a minor degree by a pressure gradient in the flow. Therefore, these approxi-

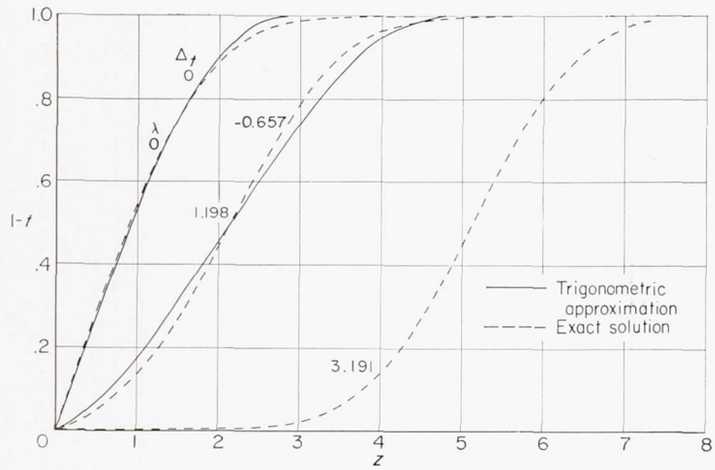

FIGURE 11.—Comparison of approximate temperature profiles for flow at stagnation point with exact solutions (ref. 14).

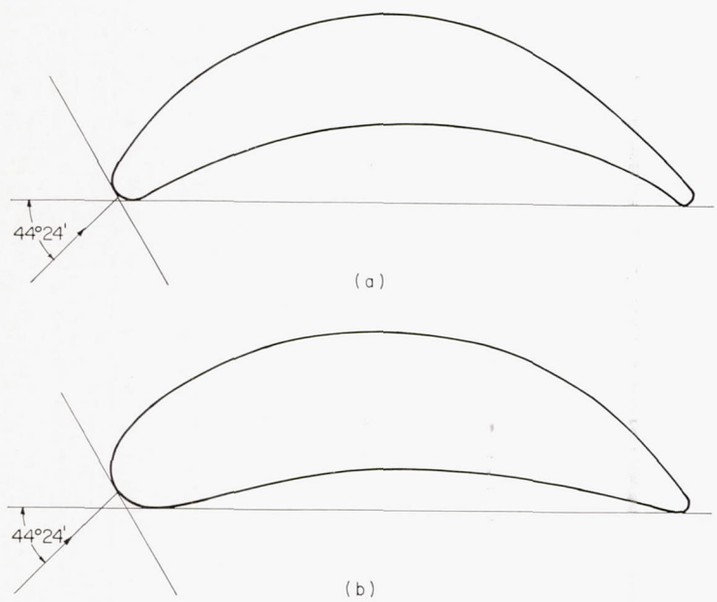

(a) Blade I. Ratio of chord length to distance between consecutive blades c/s, 1.408.

(b) Blade II. Ratio of chord length to distance between consecutive blades c/s, 1.136.

FIGURE 12.—Turbine-blade profiles used for calculated examples.

mations should be quite good for a solid surface. For a porous wall, with a constant pressure along its surface, and for a fluid with a Prandtl number of 1, the velocity and temperature profiles are again similar. Therefore, figure 10 also shows the degree of approximation for the temperature profile.

For the flow in the neighborhood of a stagnation point and a fluid with a Prandtl number of 1, some temperature profiles were calculated in reference 14. Figure 11 presents the exact temperature profiles and the approximations in a way that shows the thickness of the temperature boundary layer, which is defined in the same way as the displacement thickness, to be the same for the accurate solution and the corresponding approximation. Figure 11 shows that the agreement is satisfactory as long as the coolant flow characterized by the value λ or Δ_t is not too large. The approximation for the highest coolant flow rate (λ=3.191) is not shown since it is obvious that the exact curve cannot be approximated by the trigonometric functions from which the approximation is composed. Large coolant flows in the ranges where the agreement ceases to exist will probably not be used because the gain in cooling effect for a given increase in coolant flow is too small in this range.

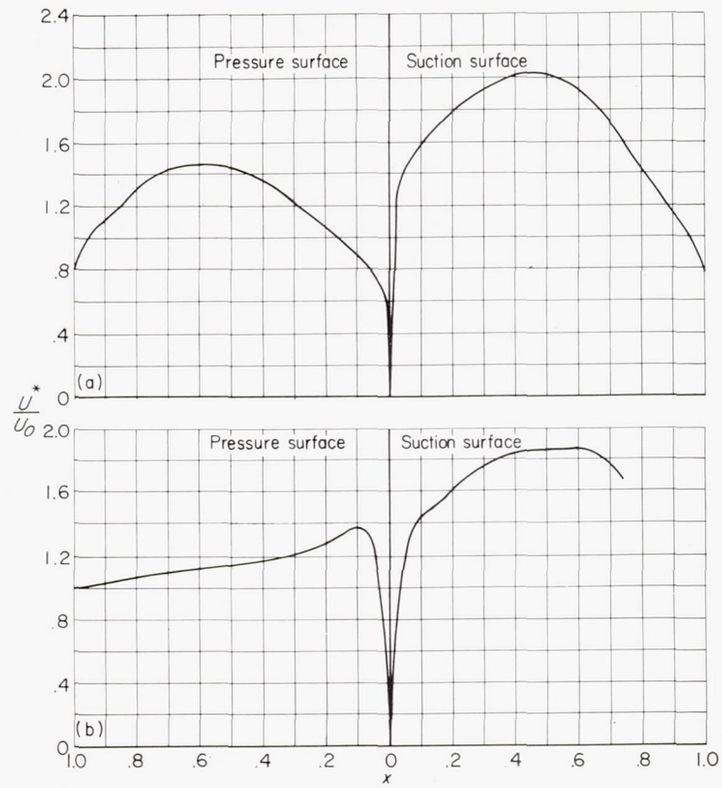

(a) Blade I.
(b) Blade II.

FIGURE 13.—Velocity distribution around surface of blade.

NUMERICAL CALCULATIONS FOR TURBINE BLADES

The method developed in the previous sections was used to calculate the local distributions of the heat-transfer coefficients for two turbine blade shapes for which the velocity distributions were known. The two blades are shown in figure 12. The line at the nose of the blade indicates the circumferential direction and the arrow, the direction of the upstream velocity. Figure 13 shows the velocity distributions around the blade circumferences. The velocity distributions around the blades were calculated using the method described in reference 17.

The method outlined in this report can be used to calculate the development of the laminar-flow boundary layer in the downstream direction up to the point of separation. In reality, at the Reynolds numbers encountered in gas-turbine engines, the boundary layer usually becomes turbulent before it reaches this point. The transition point to turbulence is determined by the pressure gradients along the blade surface, by the boundary-layer thickness, by the temperature distribution within the boundary layer, and, in addition, by the curvature of the blade surface and by the stream turbulence (ref. 18). Little quantitative knowledge

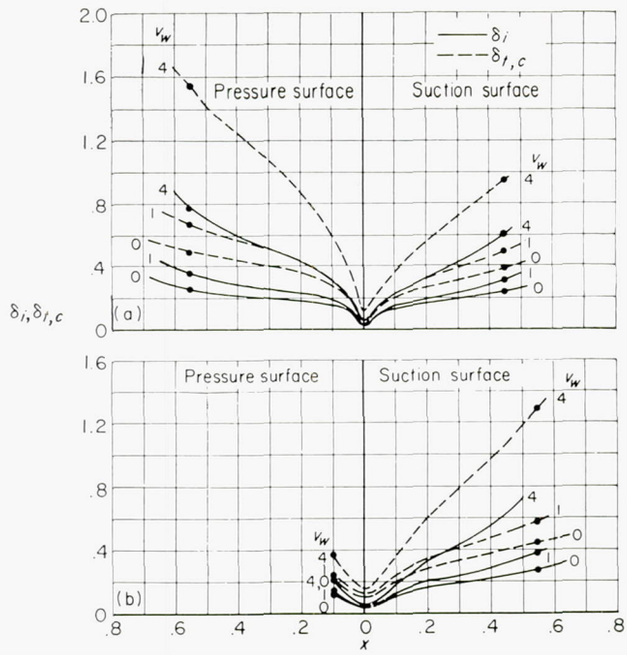

(a) Blade I.
(b) Blade II.

FIGURE 14.—Growth of flow impulse and thermal convection boundary-layer thicknesses for blade. Pr, 0.7.

exists on the influence of all these parameters. However, there are indications that on turbine blades the point of transition is near the point at which the maximum value of the velocity is reached. A calculation which deals with laminar boundary layers is therefore useful for the region near the nose of a turbine blade. The points of maximum velocity are indicated in figures 14 to 16 by small dots.

The first part of the calculation deals with the problem in which a uniform coolant flow rate v_w is prescribed along the blade periphery. The development of the flow and of the thermal boundary layers was calculated in the way described in appendix C. The results are presented in figure 14. Apparently both boundary layers start out with a finite value at the stagnation point and increase in thickness in the downstream direction on both the suction and the pressure surfaces. The boundary-layer thicknesses at any place along the blade increase with increasing coolant flow rate.

In figure 15 the local heat-transfer coefficients along the blade surfaces that are obtained from the thermal boundary-layer thickness are shown. The figures show that very high local values are encountered at the stagnation point and that the values decrease considerably with increasing distance from this point. The application of transpiration cooling decreases the heat-transfer coefficients effectively from the values obtained on a solid blade surface ($v_w=0$). The decrease is not as pronounced at the stagnation point itself as on the sides of the blade. The value of the velocity ratio v_w^*/U_0^* may be obtained from the parameter v_w presented in the diagrams by dividing it by the square root of the upstream Reynolds number. For turbine blades this Reynolds number is near the value 10^5, so that a velocity ratio $\frac{v_w^*}{U_0^*}=0.00316$ corresponds to a value of $v_w=1$. Values for this velocity ratio which are considered in practical applications are in the neighborhood of 0.01. A comparison of figures 15 (a) and (b) shows that generally the values of $Nu/\sqrt{Re_0}$ at the stagnation point decrease considerably with an increasing ratio of the radius of curvature at the blade nose to the blade chord. The values of $Nu/\sqrt{Re_0}$ are determined by the velocity gradient dU/dx, which also depends mainly on the dimensionless radius of curvature. Increasing the radius of curvature at the blade nose is therefore an effective means of decreasing the heat-transfer coefficient in this region. Downstream of the point of boundary-layer transition to turbulence, the heat-transfer coefficients will increase. To give some indication of the magnitude of the values that may be expected in the turbulent region, heat-transfer coefficients were calculated at the location $x=0.5$ under the assumption that these values are the same as on a flat plate at the same distance x from the leading edge, with a stream velocity equal to the local value found at the blade at $x=0.5$, and with an upstream Re_0 equal to 10^5. Formulas derived by Rannie and Friedman (ref. 18) were used for these calculations. The short horizontal lines in figure 15 indicate these values; the dashed part of the curve $v_w=0$ in figure 15 (a) shows the probable heat-transfer values in the transition and turbulent regions.

The surface temperature of the blade is determined by the heat-transfer coefficients. Equation (55) gives the relation between both values when heat conduction in

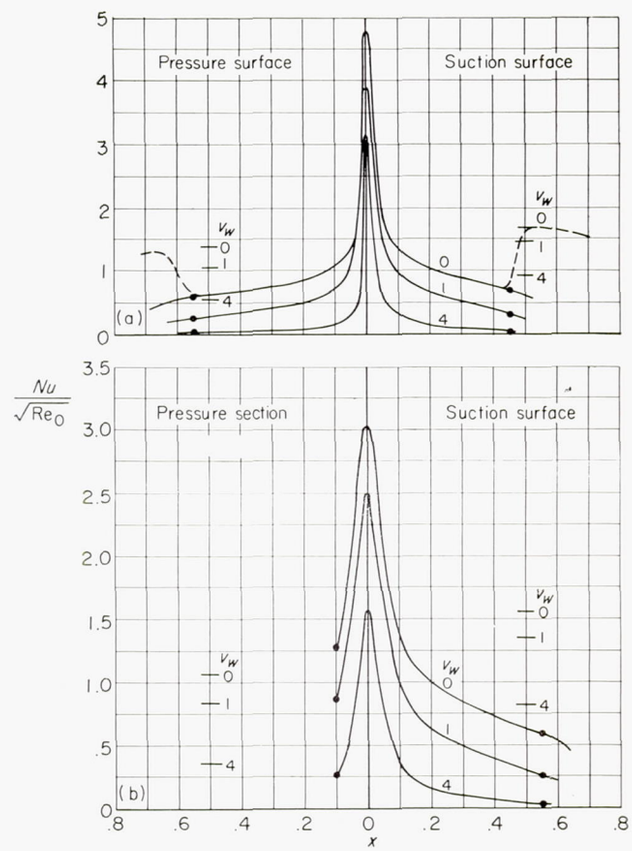

(a) Blade I.
(b) Blade II.

FIGURE 15.—Variation of local heat-transfer coefficient near stagnation point for blade. Pr, 0.7.

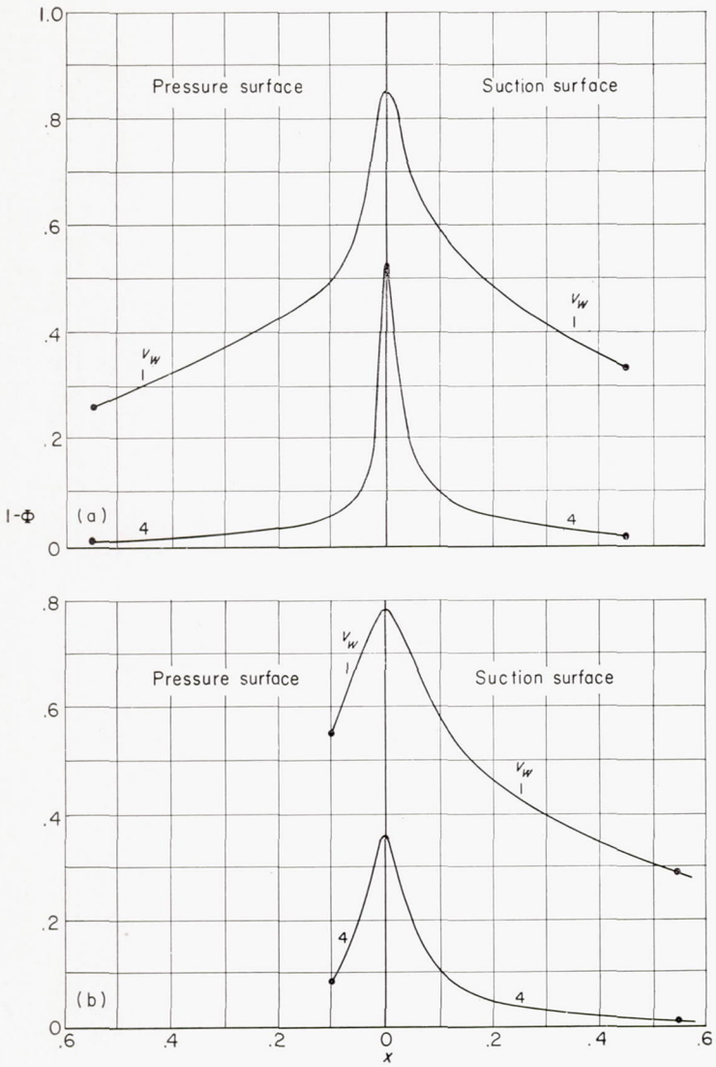

(a) Blade I.
(b) Blade II.

FIGURE 16.—Surface temperature distribution for blade. Pr, 0.7.

the blade wall and heat radiation can be neglected. Figure 16 shows the values $1-\Phi$ determined from equation (55). The quantity $1-\Phi$ is the ratio of the difference in blade surface temperature minus coolant temperature to the difference in effective gas temperature minus coolant temperature. The higher heat-transfer coefficients near the leading edge create high blade temperatures at that location. Heat conduction within the blade wall tends to reduce these high local temperatures. This reduction is assisted by the fact that the blade temperatures are especially low in the laminar region on both sides of the leading edge. Therefore, it may be that the blade-nose temperature is reduced to a value not higher than the blade-wall temperature in the turbulent part, especially for blades with a blunt nose. On the other hand, it has to be kept in mind that the heat-conductivity values for porous materials are lower than for solid walls (ref. 18). It has already been mentioned that temperature gradients along the blade surface influence the local heat-transfer coefficients somewhat; however, not enough information is available to account for this effect. A surface temperature that decreases in flow direction tends to increase the heat-transfer coefficients so that the decrease in surface temperature on both sides of the stagnation point may be slightly less than those shown in figure 16 where heat conduction within the blade walls is excluded.

A second set of calculations was made for blade I to determine that distribution of the local coolant flow rate v_w along the blade surface which results in a constant blade temperature. The procedure for such a calculation is also described in appendix C. The local coolant flow rates v_w which are necessary in order to keep the temperature ratio Φ (eq. (55)) at the value 0.7 are shown in figure 17. The flow boundary layer and the thermal boundary layer determined in this way are presented in figure 18. A comparison of this figure with figure 14(a) indicates that the development of the boundary layers is considerably different for both cases. The boundary-layer growth is smaller for the case of constant wall temperature. Figure 17 shows that the highest local flow rates are necessary near the stagnation point in order to keep the wall temperature down at that place. The

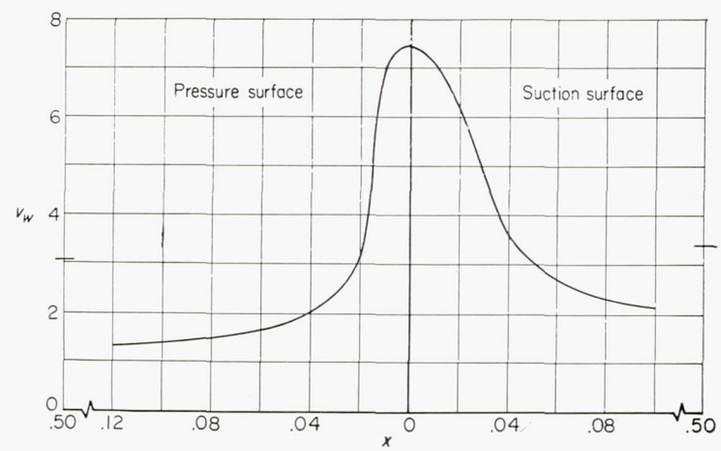

FIGURE 17.—Variation of coolant flow required to maintain constant blade temperature for blade I. Φ, 0.7; Pr, 0.7.

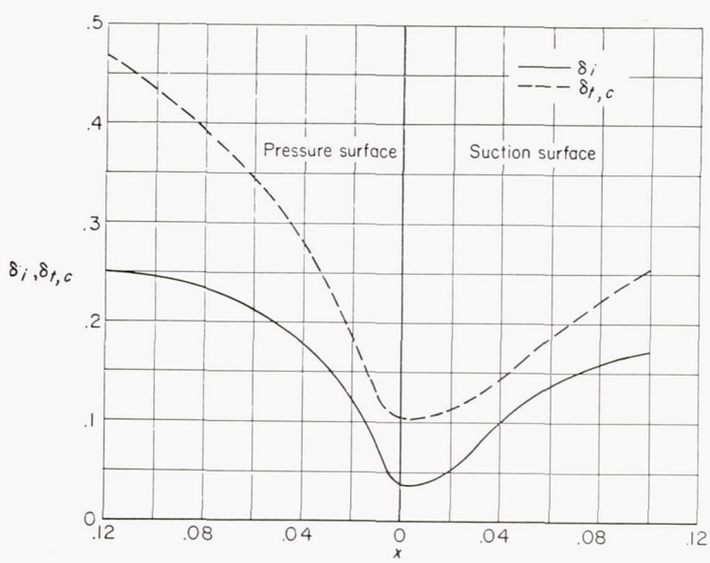

FIGURE 18.—Growth of flow impulse and thermal convection boundary-layer thicknesses for constant blade temperature for blade I. Φ, 0.7; Pr, 0.7.

magnitude of the coolant flow rate at the stagnation point is proportional to the square root of the velocity gradient dU/dx, which is itself determined mainly by the value of the radius of curvature at the blade nose. The smaller this radius, the larger the velocity gradient and the local coolant-flow rate. The flow rates decrease on both the pressure and the suction surfaces in the downstream direction. Downstream of the transition point the boundary layer will be turbulent. It is known that the cooling effectiveness of a turbulent boundary layer is less than that of a laminar boundary layer. Correspondingly higher values of the coolant flow rate are necessary in the turbulent region in order to keep the blade temperature constant. In order to give some indication of the magnitude of the coolant flow rate necessary for the turbulent region, the values v_w which result in the same value ($\Phi=0.7$) as in the laminar region were calculated at the location $x=0.5$. For this calculation the formulas presented in reference 18 were used and it was again assumed that the local Φ value on the blade surface is the same as on a flat plate at the same distance from the leading edge and with a velocity equal to the local stream velocity U and an upstream Reynolds number Re_0 equal to 10^5. The flow rates v_w obtained in this way are indicated by short horizontal lines in figure 17. The values in the turbulent region along the blade can be expected not to deviate much from these values. Apparently a considerably higher coolant flow rate is necessary in the turbulent portion of the blade surface than in most of the laminar portion. In order to simplify manufacturing problems, turbine blades may be produced in such a way that the required coolant flow rate has a constant value along the pressure surface and a different constant value along the suction surface. This then results in lower local blade temperatures in the region of laminar boundary layers; the heat conduction into this cooler part of the blade may reduce the local temperatures at the stagnation point to values equal to or lower than the temperatures in the turbulent region, especially when the radius of curvature at the blade nose is not very small. For blades with a very pointed nose it may be necessary to have a coolant flow rate at the stagnation point approximately twice as large as along the sides in order to reduce the temperature at that point.

CONCLUSIONS

A method which permits the approximate calculation of local heat-transfer coefficients and surface temperatures in the laminar flow region around cylinders of arbitrary cross section with transpiration-cooled walls was developed. Velocity and temperature profiles in the boundary layer were approximated by trigonometric expressions. The method was applied to determine local heat-transfer coefficients and surface temperatures in the laminar region of two transpiration-cooled turbine blades for a given coolant flow rate. Coolant-flow distributions necessary for maintaining uniform blade temperatures were also determined. The following conclusions are made:

1. For small coolant flow rates, the assumed trigonometric approximations for the velocity and temperature profiles within the boundary layer agree well with exact solutions. For high coolant flow rates (which are outside the range of practical interest), the agreement becomes poor. It is, however, better than the four-term polynomial approximation formerly used.

2. Transpiration cooling results in a considerable reduction in heat-transfer coefficients for turbine blades in the laminar region.

3. The surface temperatures of a blade with negligible heat conduction are highest at the leading edge, lowest in the rest of the laminar region, and have intermediate values in the turbulent region.

4. The following variation of the coolant flow rate along the blade surface is necessary to keep the blade temperature constant. Highest local coolant flow rates are required at the stagnation point in order to keep the blade surface temperature down at that point. The coolant flow rates decrease very markedly in the downstream direction on both the suction and pressure surfaces in the laminar region. However, they increase again when the turbulent region is reached.

5. In order to maintain the same surface temperature on both sides of the blade, different coolant flow rates should be used for the suction and pressure surfaces.

Lewis Flight Propulsion Laboratory
National Advisory Committee for Aeronautics
Cleveland, Ohio, *June 22, 1951*

APPENDIX A

SYMBOLS

The following symbols are used in this report:

c chord length of turbine blade, ft

c_p specific heat at constant pressure, Btu/(lb)(°F)

f_1 function of shape factor of velocity profile (see eqs. (38) and (40))

f_2 function of shape factor of velocity profile (see eqs. (39) and (41))

f_3 function of Pr, K, v_w, and δ (see eq. (46))

h heat-transfer coefficient, Btu/(sec)(sq ft) (°F)

K ratio of thermal to flow boundary-layer thickness, δ_t/δ

k thermal conductivity, Btu/(sec)(ft)(°F)

L length of either side of surface of profile measured from stagnation point, ft

m exponent (termed Euler number) in $U=U_1x^m$

Nu Nusselt number, hL/k

Pr Prandtl number, $c_p\mu/k$

p^* pressure along body, lb/sq ft

Re_0 Reynolds number, U_0L/ν

s distance between blades, ft

t temperature difference between local and free-stream values, °F

U nondimensional stream velocity, U^*/U_0

U^* stream velocity, ft/sec

U_0 upstream velocity, ft/sec

U_1 constant in wedge-flow velocity, $U=U_1x^m$

u nondimensional velocity component along surface, u^*/U_0

u^* component of velocity along surface, ft/sec

v nondimensional velocity component normal to surface, $\frac{v^*}{U_0}\sqrt{Re_0}$

v^* velocity component normal to surface, ft/sec

x nondimensional distance along surface, x^*/L

x^* distance from stagnation point along surface of profile, ft

y nondimensional distance normal to surface, $\frac{y^*}{L}\sqrt{Re_0}$

y^* distance normal to surface, ft

z nondimensional distance used in wedge-type flow, $\frac{y}{\sqrt{2-\beta}}\sqrt{\frac{U}{x}}$

z_i nondimensional displacement thickness used in wedge-type flow, $\frac{\delta_i}{\sqrt{2-\beta}}\sqrt{\frac{U}{x}}$

β shape parameter for wedge-type flow, $2m/(m+1)$

Δ shape parameter of velocity profiles (see eqs. (23) and (25))

Δ_t shape parameter of temperature profile (see eq. (28) or (48))

δ flow boundary-layer thickness

δ_d flow boundary-layer displacement thickness, $\int_0^\infty\left(1-\frac{u}{U}\right)dy$

δ_i flow boundary-layer momentum or impulse thickness, $\int_0^\infty\frac{u}{U}\left(1-\frac{u}{U}\right)dy$

δ_t thermal boundary-layer thickness

$\delta_{t,c}$ thermal boundary-layer convection thickness, $\int_0^\infty\theta\frac{u}{U}dy$

θ nondimensional temperature ratio, t/t_w

λ shape parameter for exact solutions for porous walls, $v_w\sqrt{\frac{x}{U}}$

μ viscosity, lb/(ft)(sec)

ν kinematic viscosity, μ/ρ, sq ft/sec

ρ density, lb/cu ft

Φ nondimensional temperature ratio, t_w/t_c

Subscripts:

c coolant (at blade surface)

w wall

0 upstream condition

Superscripts:

$*$ dimensional

$'$ differentiated with respect to x

APPENDIX B

DETERMINATION OF THERMAL BOUNDARY-LAYER CONVECTION THICKNESS

The determination of the thermal boundary-layer convection thickness $\delta_{t,c}$, which is similar to the impulse thickness of the flow boundary layer, results from the evaluation of equation (15)

$$\delta_{t,c}=\int_0^\infty\theta\frac{u}{U}dy \tag{15}$$

when the assumed temperature and velocity profiles are inserted in the integrand. A single temperature profile was assumed; it is given by equation (27) and is for $0\leq\frac{y}{\delta_t}\leq1$

$$\left.\begin{aligned}&\theta=1-\sin\frac{\pi}{2}\frac{y}{\delta_t}-\Delta_t\sin\frac{\pi}{2}\frac{y}{\delta_t}\left(1-\sin\frac{\pi}{2}\frac{y}{\delta_t}\right)\\&\text{and for }\frac{y}{\delta_t}\geq1\\&\theta=0\end{aligned}\right\} \tag{27}$$

Distinct velocity profiles were assumed, depending on the sign of the shape parameter Δ. Moreover, these profiles were further subdivided into different expressions depending on $\frac{y}{\delta}\leq 1$ or $\frac{y}{\delta}\geq 1$. These assumed velocity profiles are given by equations (22) and (24); they are for $\Delta\geq 0$, $0\leq\frac{y}{\delta}\leq 1$.

$$\left.\begin{aligned}&\frac{u}{U}=\sin\frac{\pi}{2}\frac{y}{\delta}+\Delta\left(1-e^{-\frac{3y}{\delta}}-\sin\frac{\pi}{2}\frac{y}{\delta}\right)\\&\text{and for }\frac{y}{\delta}\geq 1\\&\frac{u}{U}=1-\Delta e^{-\frac{3y}{\delta}}\end{aligned}\right\}\tag{22}$$

for $\Delta\leq 0$, $0\leq\frac{y}{\delta}\leq 1$

$$\left.\begin{aligned}&\frac{u}{U}=\sin\frac{\pi}{2}\frac{y}{\delta}+\Delta\sin\frac{\pi}{2}\frac{y}{\delta}\left(1-\sin\frac{\pi}{2}\frac{y}{\delta}\right)\\&\text{and for }\frac{y}{\delta}\geq 1\\&\frac{u}{U}=1\end{aligned}\right\}\tag{24}$$

It is at once obvious that, for the evaluation of $\delta_{t,c}$, four distinct cases must be considered.

The upper limit of the integral in the evaluation of $\delta_{t,c}$ may be restricted to the value δ_t by virtue of the assumed temperature profile. If $\delta_t\leq\delta$, the value of $\delta_{t,c}$ can be determined from a single integral with 0 and δ_t as limits, because the integrand vanishes for $y\geq\delta_t$. On the other hand, if $\delta<\delta_t$, two integrals are required for the evaluation of $\delta_{t,c}$ because of the assumed velocity profiles. These integrals have limits 0 and δ, and δ and δ_t.

Results of the evaluation of $\delta_{t,c}$ for the four cases follow:

Case I—$\Delta\leq 0$ **and** $\delta_t\leq\delta$:

$$\delta_{t,c}=\int_0^{\delta_t}\left[1-\sin\frac{\pi}{2}\frac{y}{\delta_t}-\Delta_t\sin\frac{\pi}{2}\frac{y}{\delta_t}\left(1-\sin\frac{\pi}{2}\frac{y}{\delta_t}\right)\right]\left[\sin\frac{\pi}{2}\frac{y}{\delta}+\Delta\sin\frac{\pi}{2}\frac{y}{\delta}\left(1-\sin\frac{\pi}{2}\frac{y}{\delta}\right)\right]dy$$

Integration and simplification lead to the following result:

$$\begin{aligned}\frac{\delta_{t,c}}{\delta}=&\frac{2}{\pi}(1+\Delta)\left(1-\cos\frac{\pi}{2}K\right)-\frac{\Delta}{2}\left(K-\frac{1}{\pi}\sin\pi K\right)+(1+\Delta+\Delta_t+\Delta\Delta_t)\left[\frac{K}{\pi(K+1)}\sin\frac{\pi}{2}(K+1)-\frac{K}{\pi(K-1)}\sin\frac{\pi}{2}(K-1)\right]+\\&(\Delta+\Delta\Delta_t)\left[\frac{K^2}{\pi(2K-1)}+\frac{K^2}{\pi(2K+1)}-\frac{K^2}{\pi(2K-1)}\cos\pi\left(K-\frac{1}{2}\right)-\frac{K^2}{\pi(2K+1)}\cos\pi\left(K+\frac{1}{2}\right)\right]+\\&(\Delta_t+\Delta\Delta_t)\left[\frac{1}{\pi(2-K)}+\frac{1}{\pi(2+K)}-\frac{2}{\pi}\cos\frac{\pi K}{2}-\frac{1}{\pi(2-K)}\cos\pi\left(1-\frac{K}{2}\right)-\frac{1}{\pi(2+K)}\cos\pi\left(1+\frac{K}{2}\right)\right]+\\&\Delta\Delta_t\left[\frac{1}{4\pi}\sin\pi K-\frac{K}{8\pi(K+1)}\sin\pi(K+1)-\frac{K}{8\pi(K-1)}\sin\pi(K-1)-\frac{K}{4}\right]\end{aligned}$$

Case II—$\Delta\leq 0$ **and** $\delta_t>\delta$:

$$\begin{aligned}\delta_{t,c}=&\int_0^{\delta}\left[1-\sin\frac{\pi}{2}\frac{y}{\delta_t}-\Delta_t\sin\frac{\pi}{2}\frac{y}{\delta_t}\left(1-\sin\frac{\pi}{2}\frac{y}{\delta_t}\right)\right]\left[\sin\frac{\pi}{2}\frac{y}{\delta}+\Delta\sin\frac{\pi}{2}\frac{y}{\delta}\left(1-\sin\frac{\pi}{2}\frac{y}{\delta}\right)\right]dy+\\&\int_{\delta}^{\delta_t}\left[1-\sin\frac{\pi}{2}\frac{y}{\delta_t}-\Delta_t\sin\frac{\pi}{2}\frac{y}{\delta_t}\left(1-\sin\frac{\pi}{2}\frac{y}{\delta_t}\right)\right](1)\,dy\end{aligned}$$

Integration and simplification in this case lead to

$$\frac{\delta_{t,c}}{\delta}=(1+\Delta)\frac{2}{\pi}-\frac{\Delta}{2}+K-1-\frac{2K}{\pi}(1+\Delta_t)\cos\frac{\pi}{2K}+\Delta_t\left(\frac{K}{2}-\frac{1}{2}+\frac{K}{2\pi}\sin\frac{\pi}{K}\right)+$$

$$(1+\Delta+\Delta_t+\Delta\Delta_t)\left\{\frac{K}{\pi(K+1)}\sin\left[\frac{\pi}{2}\frac{(K+1)}{K}\right]-\frac{K}{\pi(K-1)}\sin\left[\frac{\pi}{2}\frac{(K-1)}{K}\right]\right\}+$$

$$(\Delta+\Delta\Delta_t)\left\{\frac{K^2}{\pi(2K+1)}+\frac{K^2}{\pi(2K-1)}-\frac{K^2}{\pi(2K-1)}\cos\left[\frac{\pi(2K-1)}{2K}\right]-\frac{K^2}{\pi(2K+1)}\cos\left[\frac{\pi(2K+1)}{2K}\right]-\frac{2K}{\pi}\cos\frac{\pi}{2K}\right\}+$$

$$(\Delta_t+\Delta\Delta_t)\left\{\frac{1}{\pi(2+K)}+\frac{1}{\pi(2-K)}-\frac{1}{\pi(2-K)}\cos\left[\frac{\pi(2-K)}{2K}\right]-\frac{1}{\pi(2+K)}\cos\left[\frac{\pi(2+K)}{2K}\right]\right\}+$$

$$\Delta\Delta_t\left\{\frac{K}{4\pi}\sin\frac{\pi}{K}-\frac{1}{4}-\frac{K}{8\pi(K-1)}\sin\left[\frac{\pi(K-1)}{K}\right]-\frac{K}{8\pi(K+1)}\sin\left[\frac{\pi(K+1)}{K}\right]\right\}$$

Case III $-\Delta\geq 0$ **and** $\delta_t\leq\delta$:

$$\delta_{t,c}=\int_0^{\delta_t}\left[1-\sin\frac{\pi}{2}\frac{y}{\delta_t}-\Delta_t\sin\frac{\pi}{2}\frac{y}{\delta_t}\left(1-\sin\frac{\pi}{2}\frac{y}{\delta_t}\right)\right]\left[\sin\frac{\pi}{2}\frac{y}{\delta}+\Delta\left(1-e^{-\frac{3y}{\delta}}-\sin\frac{\pi}{2}\frac{y}{\delta}\right)\right]dy$$

Integration and simplification for this case lead to

$$\frac{\delta_{t,c}}{\delta}=(1-\Delta)\frac{2}{\pi}-(1-\Delta)\frac{2}{\pi}\cos\frac{\pi K}{2}+\Delta K+\frac{\Delta}{3}e^{-3K}-\frac{\Delta}{3}+(-1+\Delta-\Delta_t+\Delta\Delta_t)\left[\frac{K}{\pi(K-1)}\sin\frac{\pi(K-1)}{K}-\frac{K}{\pi(K+1)}\sin\frac{\pi}{2}(K+1)\right]+$$

$$(\Delta+\Delta\Delta_t)\left[\frac{2K\pi}{(36K^2+\pi^2)}-\frac{2K}{\pi}-\frac{12K^2}{(36K^2+\pi^2)}e^{-3K}\right]+(\Delta_t-\Delta\Delta_t)\left[\frac{1}{\pi(2+K)}+\frac{1}{\pi(2-K)}-\frac{1}{\pi(2-K)}\cos\pi\left(1-\frac{K}{2}\right)-\right.$$

$$\left.\frac{1}{\pi(2+K)}\cos\pi\left(1+\frac{K}{2}\right)-\frac{2}{\pi}\cos\frac{\pi K}{2}\right]+\Delta\Delta_t\left[\frac{K}{2}-\frac{\pi^2}{6(9K^2+\pi^2)}+\frac{\pi^2}{6(9K^2+\pi^2)}e^{-3K}+\frac{3K^2}{(9K^2+\pi^2)}e^{-3K}\right]$$

Case IV $-\Delta\geq 0$ **and** $\delta_t>\delta$:

$$\delta_{t,c}=\int_0^{\delta}\left[1-\sin\frac{\pi}{2}\frac{y}{\delta_t}-\Delta_t\sin\frac{\pi}{2}\frac{y}{\delta_t}\left(1-\sin\frac{\pi}{2}\frac{y}{\delta_t}\right)\right]\left[\sin\frac{\pi}{2}\frac{y}{\delta}+\Delta\left(1-e^{-\frac{3y}{\delta}}-\sin\frac{\pi}{2}\frac{y}{\delta}\right)\right]dy+$$

$$\int_{\delta}^{\delta_t}\left[1-\sin\frac{\pi}{2}\frac{y}{\delta_t}-\Delta_t\sin\frac{\pi}{2}\frac{y}{\delta_t}\left(1-\sin\frac{\pi}{2}\frac{y}{\delta_t}\right)\right]\left(1-\Delta e^{-\frac{3y}{\delta}}\right)dy$$

Integration and simplification for this case result in

$$\frac{\delta_{t,c}}{\delta}=\frac{2(1-\Delta)}{\pi}+\frac{2\Delta}{3}+K-1-(1+\Delta_t)\frac{2K}{\pi}\cos\frac{\pi}{2K}+\frac{\Delta}{3}e^{-3K}+\Delta_t\left(\frac{K}{2}-\frac{1}{2}+\frac{K}{2\pi}\sin\frac{\pi}{K}\right)+$$

$$(-1+\Delta-\Delta_t+\Delta\Delta_t)\left\{\frac{K}{\pi(K-1)}\sin\left[\frac{\pi}{2}\frac{(K-1)}{K}\right]-\frac{K}{\pi(K+1)}\sin\left[\frac{\pi}{2}\frac{(K+1)}{K}\right]\right\}+$$

$$(\Delta+\Delta\Delta_t)\left[\frac{2K\pi}{(36K^2+\pi^2)}-\frac{2K}{\pi}+\frac{2K}{\pi}\cos\frac{\pi}{2K}-\frac{12K^2}{(36K^2+\pi^2)}e^{-3K}\right]+$$

$$(\Delta_t-\Delta\Delta_t)\left[\frac{1}{\pi(2+K)}+\frac{1}{\pi(2-K)}-\frac{1}{\pi(2-K)}\cos\frac{\pi(2-K)}{2K}-\frac{1}{\pi(2+K)}\cos\frac{\pi(2+K)}{2K}\right]+$$

$$\Delta\Delta_t\left[\frac{1}{2}-\frac{K}{2\pi}\sin\frac{\pi}{K}-\frac{\pi^2}{6(9K^2+\pi^2)}+\frac{3K^2}{(9K^2+\pi^2)}e^{-3K}+\frac{\pi^2}{6(9K^2+\pi^2)}e^{-3K}\right]$$

APPENDIX C

PROCEDURE FOR CALCULATION OF FLOW AND THERMAL BOUNDARY LAYERS

In this appendix the procedure will be explained by which the flow and thermal boundary layers, the heat-transfer coefficients, and the temperature distribution around a body of given shape may be obtained. As outlined previously, the boundary conditions on the surface of the body may be prescribed in two different ways, either by prescribing the coolant velocity v_w^* or by prescribing the temperature around the surface. The calculation procedure becomes simpler in the first case and this will be considered first. In addition to the value v_w^*, the distribution of the stream velocity U^* just outside the boundary layer around the body must be known. This velocity distribution may be obtained by any of the known calcula-

tion procedures for frictionless flow on bodies without flow separation or it has to be determined experimentally when flow separation occurs. From the velocity $U^*(x)$ the gradient $U^{*\prime}(x)$ can be found.

The values mentioned have to be transformed into the dimensionless quantities $U(x)$, $U'(x)$, and v_w by use of equations (4).

FLOW BOUNDARY LAYER

The aim of this calculation is to determine the momentum thickness δ_i as a function of the distance x from the stagnation point as measured along the surface of the body.

As a first step, the value δ_i has to be found at the stagnation point. For this purpose, determine v_w^2/U', and read the value $U'\delta_i^2$ from figure 4, thereby determining the momentum thickness δ_i. The intersection of $U'\delta_i^2$ with the stagnation line in figure 3 determines Δ, the shape parameter for the velocity profile. The velocity profile itself may be determined from equation (22) or equation (24) if it is desired. The required parameters may also be taken from table I.

The momentum thickness along the profile surface is found from equation (37). This first-order linear differential equation may be solved by any of the known procedures. The method of isoclines was used for the solution of the numerical examples described previously, and its use will be outlined here. Equation (37) determines the direction of the tangents to the different δ_i^2 curves which satisfy this equation. The task is to find the one curve which contains the δ_i value calculated previously for the stagnation point. Figure 19 shows the δ_i^2 values as ordinate and the distance x from the stagnation point as abscissa. The directions of the tangents may be obtained from equation (37) for any point in this figure characterized by a pair of values x and δ_i^2 and may be inserted on the ordinates through a chosen sequence of distances x_1, x_2, x_3 . . . along the abscissa for several δ_i^2 values. The calculation proceeds for x and a chosen δ_i in the following way: determine $U'\delta_i^2$ and $v_w\delta_i$ and read from figure 3 the value Δ and from figure 2, f_1 and f_2. Calculate from equation (37), $d(\delta_i^2)/dx$. Now the direction of the tangent may be inserted in figure 19. The same calculation is repeated for other δ_i^2 values and the corresponding directions of the tangents are inserted in figure 19. The same calculation is repeated for the distances x_2, x_3 . . . If the distance between these values is chosen small enough, a curve that starts out with the predetermined value δ_i^2 at the stagnation point and is tangent to the straight lines inserted in figure 19 can be drawn in the figure with good accuracy. The calculation may be shortened considerably when the curve is inserted step by step after the tangents have been calculated for any value x. Then the correct value δ_i^2 for the following distance x may be guessed from the shape of the curve up to that point and the tangents need to be calculated only in the neighborhood of this value.

The values which will be needed for the calculation may be arranged in a table such as the following:

x	U	U'	v_w	δ_i	Δ	δ
0						
x_1						
x_2						

The momentum thickness δ_i in this table results from the preceding calculation. The shape parameter Δ was found in the course of this calculation and the value δ may be determined from figure 2.

THERMAL BOUNDARY LAYER

The calculation now has to be restricted to a fluid with a certain Prandtl number. The value which characterizes the thermal boundary layer and will be determined in this section is the convection boundary-layer thickness $\delta_{t,c}$. To find this-

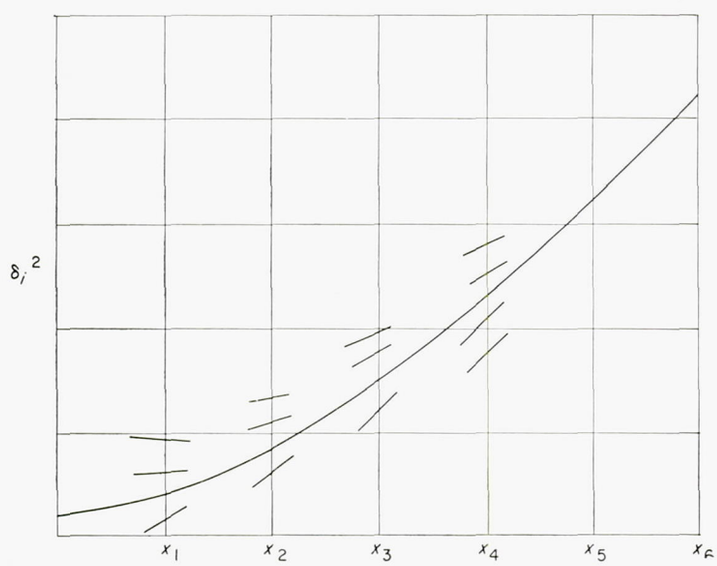

FIGURE 19.—Isocline solution of flow boundary-layer equation.

value at the stagnation point, determine $v_w\delta_i$ from the preceding table, read from figure 7 or table II $\delta_{t,c}/\delta$ and f_3. This determines $\delta_{t,c}$. Equation (52) determines the local Nusselt number Nu, and for the case in which the heat-balance equation (54) is satisfied, equation (55) determines also the temperature ratio Φ. The shape factor Δ_t determining the shape of the temperature profile according to equation (27) may be determined from figure 5 and equation (48).

The convection boundary-layer thickness along the surface of the profile is determined by equation (46). This equation may be solved in the same way as the corresponding flow equation. Figure 20 indicates the procedure. The product $U\delta_{t,c}$ is plotted over the distance x from the stagnation point. The short straight lines in the figure again indicate the direction of the tangents. It is known from exact solutions that the gradient of any boundary-layer thickness at the stagnation point is zero and that the boundary-layer thickness itself has a finite value. Thus, the curve $U\delta_{t,c}$ in figure 20 starts out with the value zero and with the inclination $U'\delta_{t,c}$ for $x=0$. In order to find the direction of the tangents for any value x, for example x_1, assume a value $U\delta_{t,c}$, calculate $\delta_{t,c}$ and $\delta_{t,c}/\delta$, read the value K from figure 6, determine the product $Pr\ v_w\delta K$, read f_3 from figure 5, and calculate from the heat-flow equation (46) the gradient $\frac{d}{dx}(U\delta_{t,c})$. Insert the corresponding tangent into figure 20 and repeat the calculation for other values $U\delta_{t,c}$. Now the curve $U\delta_{t,c}$, which begins with the value zero for $x=0$ and with the corresponding inclination, may be extended to x_1. The calculation is now repeated for the next distance x_2, the curve is extended, and this procedure is repeated until the curve is known for the whole length x. The result of this calculation gives $\delta_{t,c}$ and f_3. These values may be inserted in a table such as the following:

x	$\delta_{t,c}$	f_3	$\frac{Nu}{\sqrt{Re_0}}$	Φ
x_1				
x_2				
x_3				

The ratio $Nu/\sqrt{Re_0}$, which characterizes the local heat-transfer coefficient, is found from equation (52). For the special case that the heat-balance equation (54) is fulfilled, equation (55) determines the temperature ratio Φ.

FIGURE 20.—Isocline solution of thermal boundary-layer equation.

The calculation is more tedious when the surface temperature instead of the flow velocity v_w is prescribed along the blade. When the heat-balance equation (54) is satisfied, the temperature ratio Φ may be determined as a function of x. Now the momentum equation (37) and the heat-flow equation (46) have to be solved simultaneously by a trial-and-error procedure. A value v_w is assumed. The calculation procedure described previously is carried out to determine a temperature ratio Φ corresponding to the assumed v_w. The calculation has to be repeated until the determined Φ value matches the prescribed value. This calculation has to be carried out stepwise for the distances x_1, x_2, x_3, . . .

In some cases heat may be transferred to the surface of the profile by radiation and may flow along the wall of the body by conduction. Then an equation which takes these processes into account has to replace the equation (54). The determination of the coolant flow velocity v_w, which results in a prescribed blade surface temperature, may be determined in the same way as was just described. The procedure, however, becomes rather tedious in this case.

REFERENCES

1. Eckert, E.: Die Berechnung des Wärmeübergangs in der laminaren Grenzschicht umströmter Körper. VDI Forschungsheft 416, Bd. 13, Sept.-Oct., 1942.
2. von Kármán, Th.: On Laminar and Turbulent Friction. NACA TM 1092, 1946.
3. Pohlhausen, K.: Zur näherungsweisen Integration der Differentialgleichung der laminaren Grenzschicht. Z.a.M.M., Bd. 1, Heft 4, Aug. 1921, pp. 252–268.
4. Walz, A.: Application of Wieghardt's Energy Theorem to Velocity Profiles of One Parameter in Laminar Boundary Layers. Rep. and Trans. No. 230, British M.A.P., Sept. 15, 1946.
5. Tetervin, Neal, and Lin, Chia Chiao: A General Integral Form of the Boundary-Layer Equation for Incompressible Flow with an Application to the Calculation of the Separation Point of Turbulent Boundary Layers. NACA TN 2158, 1950.
6. Schlichting, H.: An Approximate Method for Calculation of the Laminar Boundary Layer with Suction for Bodies of Arbitrary Shape. NACA TM 1216, 1949.
7. Dorodnitzyn, A.: Laminar Boundary Layer in Compressible Fluid. Comptes Rendus, vol. XXXIV, no. 8, 1942, pp. 213–219.
8. Dienemann, W.: Calculation of the Thermal Boundary Layer of a Body in Incompressible Laminar Flow. Jour. Aero. Sci., vol. 18, no. 1, Jan. 1951, pp. 64–65.
9. Goland, Leonard: A Theoretical Investigation of Heat Transfer in the Laminar Flow Regions of Airfoils. Jour. Aero. Sci., vol. 17, no. 7, July 1950, pp. 436–440.
10. Yuan, Shao Wen: Heat Transfer in Laminar Compressible Boundary Layer on a Porous Flat Plate with Fluid Injection. Jour. Aero. Sci., vol. 16, no. 12, Dec. 1949, pp. 741–748.
11. Schuh, H.: Boundary Layers of Temperature. Reps. & Trans. No. 1007, AVA Monographs, British M. A. P., Apr. 15, 1948.
12. Seban, R. A., Drake, R. M., and Levy, S.: Heat Transfer to Laminar Boundary Layers Under Variable Free Stream Pressure Conditions. Prog. Rep. No. 1, ser. 1, issue 1, Eng. Dept., Univ. Calif. (Berkeley), Oct. 12, 1950. (Contract AF–33(038)–12941, UCB–96439.)
13. Chapman, Dean R., and Rubesin, Morris W.: Temperature and Velocity Profiles in the Compressible Laminar Boundary Layer with Arbitrary Distribution of Surface Temperature. Jour. Aero. Sci., vol. 16, no. 9, Sept. 1949, pp. 547–565.
14. Eckert, E. R. G.: Heat Transfer and Temperature Profiles in Laminar Boundary Layers on a Sweat-Cooled Wall. Tech. Rep. No. 5646, Air Materiel Command, Nov. 3, 1947.
15. Brown, W. Byron: Exact Solutions of the Laminar Boundary Layer Equations for a Porous Plate with Variable Fluid Properties and a Pressure Gradient in the Main Stream. A.S.M.E. Proc. First U. S. Nat. Cong. Appl. Mech., pub. by A.S.M.E., 1952, pp. 843–852.
16. Hartree, D. R.: On an Equation Occurring in Falkner and Skan's Approximate Treatment of the Equations of the Boundary Layer. Proc. Cambridge Phil. Soc., vol. 33, pt. 2, Apr. 1937, pp. 223–239.
17. Katzoff, S., Finn, Robert S., and Laurence, James C.: Interference Method for Obtaining the Potential Flow Past an Arbitrary Cascade of Airfoils. NACA Rep. 879, 1947. (Supersedes NACA TN 1252.)
18. Eckert, E. R. G., and Esgar, Jack B.: Survey of Advantages and Problems Associated with Transpiration Cooling and Film Cooling of Gas-Turbine Blades. NACA RM E50K15, 1951.

TABLE I—STAGNATION POINT VALUES FOR FLOW BOUNDARY LAYER

$v_w\delta_i$	Δ	$U'\delta_i^2$	$\frac{\delta_i}{\delta}$	$\frac{\delta_d}{\delta}$	f_1	f_2	$v_w\delta$
−0. 4999	1. 0000	0. 0001	0. 1667	0. 3333	4. 0000	0. 5000	−2. 9988
−. 4	0. 78	. 0008	. 1614	. 3399	4. 1059	. 4336	−2. 4783
−. 3	. 6065	. 01935	. 1567	. 3452	4. 2029	. 3820	−1. 9145
−. 2	. 486	. 0345	. 1532	. 3488	4. 2768	. 3471	−1. 3055
−. 1	. 411	. 05225	. 1509	. 3510	4. 3260	. 3257	−0. 6627
0	. 359	. 0715	. 1492	. 3526	4. 3633	. 3110	0
. 05	. 329	. 0812	. 1484	. 3533	4. 3800	. 3050	. 3380
. 1	. 3075	. 09025	. 1475	. 3541	4. 4007	. 2966	. 6780
. 2	. 279	. 1105	. 1466	. 3550	4. 4216	. 2888	1. 3643
. 3	. 242	. 130	. 1453	. 3561	4. 4508	. 2785	2. 0647
. 4	. 225	. 151	. 1447	. 3566	4. 4644	. 2739	2. 7643
. 5	. 208	. 1718	. 1441	. 3571	4. 4781	. 2692	2. 4698
. 6	. 1835	. 19175	. 1433	. 3579	4. 4976	. 2627	4. 1870
. 7	. 172	. 213	. 1429	. 3582	4. 5066	. 2596	4. 8985
. 8	. 161	. 234	. 1425	. 3585	4. 5158	. 2566	5. 6140
. 9	. 151	. 255	. 1421	. 3588	4. 5250	. 2539	6. 3336
1. 0	. 142	. 276	. 1418	. 3591	4. 5324	. 2515	7. 0522
1. 1	. 135	. 2975	. 1416	. 3593	4. 5374	. 2497	7. 7684
1. 2	. 128	. 3195	. 1413	. 3595	4. 5442	. 2478	8. 4926
1. 3	. 123	. 341	. 1411	. 3597	4. 5492	. 2464	9. 2133
1. 4	. 114	. 362	. 1408	. 3599	4. 5561	. 2449	9. 9432
1. 5	. 113	. 384	. 1408	. 3600	4. 5568	. 2439	10. 6534
1. 6	. 107	. 405	. 1406	. 3602	4. 5618	. 2424	11. 3798
1. 7	. 101	. 426	. 1403	. 3604	4. 5688	. 2406	12. 1169

TABLE II—STAGNATION POINT VALUES FOR THERMAL BOUNDARY LAYER

$v_w\delta_i$	$Pr=0.7$			$Pr=1$			$Pr=2$			$Pr=10$		
	K	$\frac{\delta_{t,c}}{\delta}$	f_3	K	$\frac{\delta_{t,c}}{\delta}$	f_3	K	$\frac{\delta_{t,c}}{\delta}$	f_3	K	$\frac{\delta_{t,c}}{\delta}$	f_3
0	1. 80	0. 3888	∞	1. 56	0. 3140	∞	1. 2	0. 2042	∞	0. 66	0. 0742	∞
0. 05	1. 76	. 3949	4. 40	1. 54	. 3271	3. 610	1. 215	. 2286	2. 5448	. 78	. 1207	1. 317
. 1	1. 72	. 4142	2. 555	1. 55	. 3477	2. 113	1. 26	. 2616	1. 607	. 94	. 1773	1. 081
. 2	1. 74	. 4291	1. 629	1. 58	. 3808	1. 408	1. 35	. 3172	1. 198			
. 3	1. 74	. 4518	1. 336	1. 61	. 4124	1. 233	1. 43	. 3664	1. 091			
. 4	1. 74	. 4690	1. 228	1. 64	. 4371	1. 142	1. 50	. 4027	1. 053			
. 5	1. 74	. 4869	1. 158	1. 66	. 4607	1. 096	1. 57	. 4338	1. 0325			
. 6	1. 75	. 4995	1. 116	1. 68	. 4783	1. 068						
. 7	1. 78	. 5101	1. 087	1. 70	. 4933	1. 053						
. 8	1. 79	. 5208	1. 068	1. 72	. 5066	1. 040						
. 9	1. 80	. 5295	1. 056	1. 74	. 5174	1. 032						
1. 0	1. 80	. 5371	1. 048	1. 76	. 5266	1. 025						
1. 1	1. 84	. 5444	1. 038									
1. 2	1. 84	. 5488	1. 037									
1. 3	1. 84	. 5524	1. 028									
1. 4	1. 85	. 5569	1. 024									
1. 5	1. 85	. 5608	1. 021									
1. 6	1. 85	. 5667	1. 018									
1. 7	1. 85	. 5697	1. 017									

U. S. GOVERNMENT PRINTING OFFICE: 1957